

Phase transitions and molecular dynamics in the cyclohexane/thiourea inclusion compound

A. Desmedt,¹ S. J. Kitchin,² F. Guillaume,¹ M. Couzi,¹ K. D. M. Harris,² and E. H. Bocanegra³¹*Laboratoire de Physico-Chimie Moléculaire, UMR no. 5803 CNRS, Université de Bordeaux I, 351 cours de la Libération, F-33405 Talence, France*²*School of Chemistry, University of Birmingham, Edgbaston, Birmingham, B15 2TT, United Kingdom*³*Departamento de Física Aplicada II, Facultad de Ciencias, Universidad del País Vasco, 48080 Bilbao, Spain*

(Received 13 November 2000; revised manuscript received 30 March 2001; published 17 July 2001)

In thiourea inclusion compounds the host structure comprises a hydrogen bonded arrangement of thiourea molecules and contains unidirectional, nonintersecting channels within which guest molecules are located. Structural and dynamic properties of the cyclohexane/thiourea inclusion compound have been studied previously by a wide range of experimental techniques, providing contradictory interpretations. This organic composite crystal displays three thermotropic structural phases on cooling from room temperature, denoted phase I (rhombohedral), phase II (monoclinic), and phase III (monoclinic). However, until now, there has been no attempt to understand the relationship between the dynamics of the guest molecules and the structural and symmetry properties of the composite inclusion compound in the three phases. In the first part of this paper, we determine the space group of each phase from powder x-ray diffraction data. From this knowledge of the symmetry properties of each phase, the phase transitions are described in terms of order parameters defined on the basis of the symmetry principles of Landau theory. Theoretical analysis of the crystal strain occurring at the phase transitions allows a direct comparison between the experimental temperature dependence of the lattice parameters and predictions derived from Landau theory. In the second part of this paper, we report results from powder and single-crystal ²H NMR spectroscopy on samples of cyclohexane/thiourea containing perdeuterated cyclohexane guest molecules (C₆D₁₂). These ²H NMR experiments have shown that in phase I, the motionally averaged quadrupole coupling tensor is axially symmetric. On passing from phase I to phase II, the threefold symmetry axis of the $R = \bar{3}c$ space group of phase I is lost, such that the motionally averaged quadrupole interaction tensor is not axially symmetric in phase II. The single crystal ²H NMR spectra probe very precisely the relative orientations of the guest molecules, which are consistent with the site symmetry properties of the structure and proposed modes of crystal twinning, and demonstrate that there is only one type of dynamic species of guest molecule in phase II. In phase III, a greater degree of orientational ordering of the cyclohexane molecules is evident. From a detailed consideration of the symmetry properties of the inclusion compound, the dynamics of the guest molecules may be described using simple jump models (i.e., multidimensional pseudospin models) in all three phases. Using these models, the temperature dependence of the order parameter components has been established. These results, in conjunction with x-ray diffraction, provide important information needed to propose a microscopic model for the mechanisms of the phase transitions in the cyclohexane/thiourea inclusion compound.

DOI: 10.1103/PhysRevB.64.054106

PACS number(s): 64.60.-i, 61.50.Ks, 61.10.Nz, 64.70.Kb

I. INTRODUCTION

Crystalline organic inclusion compounds in which the host substructure forms one-dimensional channels densely loaded with guest molecules exhibit a wide range of interesting and important fundamental physicochemical properties, as illustrated, for example, by the urea and thiourea families of inclusion compounds.¹ Recently, a substantial amount of research has focused on the structural and dynamic properties and the phase transition mechanisms in the incommensurate inclusion compounds of urea,¹⁻⁸ but substantially less is known about the corresponding properties of thiourea inclusion compounds and other families of solid organic inclusion compounds. In thiourea inclusion compounds, a hydrogen bonded arrangement of thiourea molecules forms a crystalline “host” structure that has unidirectional, nonintersecting channels. Suitable “guest” molecules are located inside these channels, and examples are branched hydrocarbons, cyclohexane and certain of its derivatives and small organometallic molecules such as ferrocene. For most guest

molecules (particularly those with fairly isotropic molecular shape), the host structure is rhombohedral at ambient temperature and the guest molecules are orientationally disordered. In many cases, this rhombohedral structure transforms to a monoclinic structure at low temperature. In general, thiourea inclusion compounds have a commensurate relationship between the periodicities of the host and guest substructures along the channel direction, with two guest molecules per unit repeat distance of the thiourea host structure along the channel and a guest/thiourea molar ratio of 1/3.

Our aim is to elaborate the methodology for elucidating the phase transition mechanisms in thiourea inclusion compounds. In this paper, experimental results obtained by means of differential scanning calorimetry, x-ray diffraction, and ²H NMR spectroscopy are used as a basis for the symmetry analysis and the microscopic modeling of the structural changes. For this work, we have chosen the cyclohexane/thiourea inclusion compound C₆H₁₂/SC(NH₂)₂ as it is perhaps the prototypical member of the thiourea family of inclusion compounds. In early studies,^{9,10} three distinct

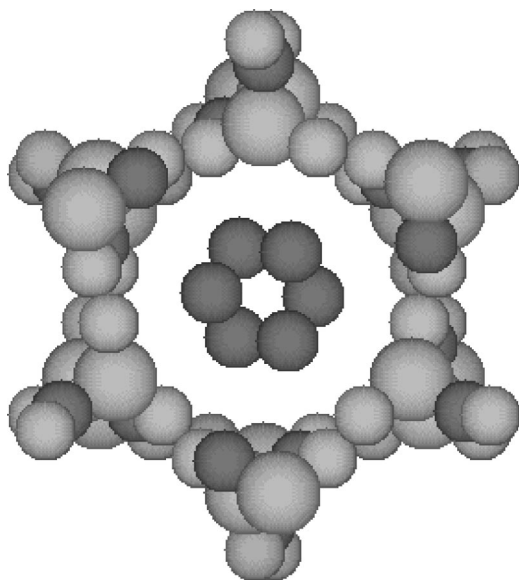


FIG. 1. View along the channel axis of the cyclohexane/thiourea inclusion compound. For clarity, hydrogen atoms are not drawn, and the cyclohexane guest molecule is shown in an arbitrary position.

thermotropic structural phases of cyclohexane/thiourea were identified. Single-crystal x-ray diffraction has shown that, at room temperature (phase I), the host substructure in cyclohexane/thiourea is the conventional rhombohedral thiourea channel structure with space group $R\bar{3}c$ (Ref. 10) (Fig. 1), and this phase exists down to 149 K. Phase II (149–129 K) is monoclinic with twice the volume of the rhombohedral unit cell and phase III (below 129 K) is also monoclinic.⁹ The space groups of the low-temperature phases II and III were not determined in these studies.

The first part of this paper is devoted to a detailed characterization of the two phase transitions in the cyclohexane/thiourea inclusion compound by means of differential scanning calorimetry and powder x-ray diffraction. The fundamental starting information that we require is to determine the space groups of the three structural phases. Here we have approached this issue using powder x-ray diffraction in preference to single-crystal x-ray diffraction, on the recognition that, in the absence of external stress, phase transitions related to a change of the crystal system (rhombohedral-monoclinic in the present case), are unavoidably associated with multiple crystal twinning¹¹ (ferroelastic domains) generally causing problems in the application of single-crystal diffraction techniques to probe the structural properties of the low-temperature phases.¹² On the other hand, the introduction of crystal twinning in the low temperature phases does not pose intrinsic problems with regard to the analysis and interpretation of powder diffraction data.

The structural transitions are then described in terms of order parameters defined on the basis of the symmetry principles of Landau theory. Then, by theoretical analysis of the crystal strain occurring at the phase transitions, we compare the experimental temperature dependence of the lattice pa-

rameters with the classical interpretation derived from Landau theory.

In the second part of this paper we investigate the dynamic properties of the cyclohexane guest molecules within the thiourea host structure and the relationship between these dynamic properties and the symmetry properties of the three phases of the composite crystal. Early studies^{9,13} of the dynamic properties of the guest molecules in the cyclohexane/thiourea inclusion compound focused on wide-line ¹H NMR spectroscopy of cyclohexane/thiourea-*d*₄ [i.e., C₆H₁₂/SC(ND₂)₂], and concluded that the guest molecules are mobile in all three phases above about 100 K. Models for the motions in each phase were proposed, but the level of detail concerning dynamic models that can be established from these experiments is considerably less than that established from subsequent ²H NMR experiments. Meirovitch *et al.*¹⁴ reported ²H NMR studies of cyclohexane-*d*₁₂/thiourea [i.e., C₆D₁₂/SC(NH₂)₂] between 134 and 345 K. On the basis of an improved experimental approach, these early ²H NMR studies were subsequently reinvestigated.¹⁵ In these studies, three dynamic regimes of the guest molecules were identified between 93 and 333 K, correlating well with the three phases discussed above. In phase III, it was shown that each cyclohexane guest molecule reorients about its threefold symmetry axis, and from ²H NMR spin-lattice relaxation time data, this motion was assigned as a threefold jump process. Changes in the dynamics of the guest molecules in phase II were ascribed to the existence of three dynamically distinct guest species (denoted A, B, and C), with the relative populations of these species changing continuously on increasing temperature. The dynamic properties of the predominant species (A) in the low-temperature region of phase II were concluded to be similar to those for phase III, whereas the dynamics of the predominant species (C) in the high-temperature region of phase II were concluded to be similar to those for phase I (described below). At intermediate temperatures in phase II, the dynamics of the predominant guest species (B) were described as rapid reorientation about the threefold symmetry axis of the guest molecule, together with rapid “wobbling within a biaxial potential of the host channels.”¹⁵ In phase I, there is extensive dynamic disorder of the guest molecules, including cyclohexane ring inversion at higher temperatures in phase I. The proposal of Poupko *et al.*¹⁵ that in phase II there is coexistence of three different types of cyclohexane molecule with markedly different dynamic properties (at a given temperature) is puzzling, particularly in view of the fact that all guest molecules in the inclusion compound have an identical (average) environment in the crystal structure.

We have exploited the fact that thiourea inclusion compounds form large single crystals with well-defined morphology to carry out single crystal ²H NMR experiments. It is well known that ²H NMR is a very sensitive probe of reorientational dynamics of the deuterated component of the system (in this case, the cyclohexane guest molecules), particularly when measurements are made on oriented single crystals. In this paper, we demonstrate that simple dynamic models may be used successfully to interpret the experimental ²H NMR spectra for the three structural phases of the

cyclohexane/thiourea inclusion compound. Furthermore, the experimental data are used to derive information on the order parameters that drive the phase transitions.

II. EXPERIMENTAL

A. Sample preparation

Crystals of the cyclohexane/thiourea and cyclohexane- d_{12} /thiourea inclusion compounds were obtained by slowly cooling solutions containing thiourea and cyclohexane (or cyclohexane- d_{12}) in methanol. The temperature was decreased systematically from 55 °C to ambient temperature over a period of two days for obtaining small single crystals and over a period of one week for obtaining large single crystals. Needle-shaped crystals were obtained, with diameter varying between approximately 1 and 6 mm and with typical length around 10 mm. The crystals were stored in the crystallization solution at ambient temperature (note that slow decomposition of the inclusion compound may occur over prolonged periods of time under normal atmospheric conditions) and were removed from this solution (and washed with methanol) only immediately prior to each experiment. Viewed along the long axis of the needle morphology (thiourea channel axis), the cross section of the crystal morphology is hexagonal. Single crystal x-ray diffraction experiments have shown that the twofold symmetry axes of phase I are perpendicular to the faces of the hexagonal crystal morphology.

B. Differential scanning calorimetry

Differential scanning calorigrams were recorded for ground powder samples on a Perkin-Elmer DSC-7 instrument. The samples were subjected to a cycle of cooling and heating between 298 and 103 K at a cooling/heating rate of 10 K min⁻¹.

C. Powder x-ray diffraction

A first set of powder x-ray diffraction patterns of the cyclohexane/thiourea inclusion compound was recorded as a function of temperature on a conventional laboratory diffractometer (Siemens D5005) using $\text{CuK}\alpha$ radiation and operating in reflection mode. Each powder diffraction pattern was recorded in the range $5^\circ \leq 2\theta \leq 40^\circ$ with a step size of 0.036° and a counting time of 4 s per step. The temperature was controlled by a helium cryostat with an accuracy of approximately 0.1 K. Powder diffraction patterns were recorded between 30 and 250 K, with emphasis on temperatures in phase II and near to each phase transition temperature. Although the phase transitions were clearly identified, the resolution was not sufficient to allow a detailed interpretation of the structural changes in the low-temperature phases in terms of space group determination. For this reason, synchrotron x-ray powder diffraction studies were performed on station 2.3 at the Synchrotron Radiation Source, Daresbury Laboratory. For these experiments, a finely ground sample of cyclohexane/thiourea was placed in a capillary sample holder sealed with a polymer film. Powder diffraction patterns were recorded in transmission geometry in the range $5^\circ \leq 2\theta \leq 70^\circ$

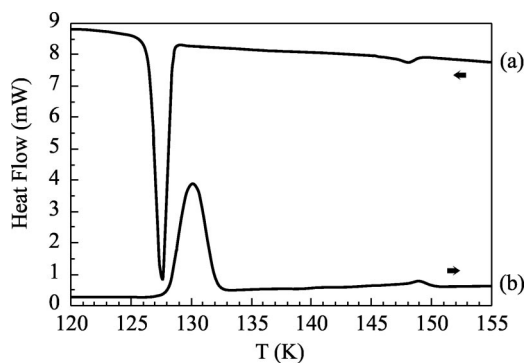


FIG. 2. Differential scanning calorigrams for the cyclohexane/thiourea inclusion compound on (a) cooling from 298 to 103 K and (b) warming from 103 to 298 K.

with a step size of 0.01° and a counting time of 4 s per step. Powder diffraction patterns were recorded at one temperature in each phase (295, 140, and 100 K). The x-ray wavelength was 1.40 Å for the experiments at 293 and 140 K, and 1.30 Å for the experiment at 100 K. The same powder sample was used to record the data for phases I and II, whereas a fresh sample was used to record the data for phase III. We note that a powder diffraction pattern was recorded at room temperature on the sample used for phase III for comparison with the sample used for phases I and II, confirming that the samples used in each case were identical.

D. ^2H NMR spectroscopy

All ^2H NMR experiments were carried out on a Chemagnetics CMX300 Infinity spectrometer (^2H operating frequency 46.080 MHz). Spectra were recorded using the standard quadrupole echo pulse sequence $[(\pi/2)_\phi - \tau_1 - (\pi/2)_{\phi \pm \pi/2} - \tau_2 - \text{acquire} - \text{recycle}]$ with an eight-step phase cycle.¹⁶ Typically 1000 transients were acquired for each spectrum, with separate spectra recorded for echo delays (τ_1) of 30 and 150 μs . The recycle delays were set to at least five times the largest value of T_1 at each temperature. The stability of the temperature controller was estimated to be better than around ± 1 K. ^2H NMR spectra on powder samples were recorded in the temperature range 127 to 297 K using a static probe with 5 mm diameter coil. Single crystal ^2H NMR experiments were carried out using a Chemagnetics goniometer probe (with 5 mm diameter coil), allowing reorientation of the crystal about an axis perpendicular to \vec{B}_0 . The needle-shaped single crystal was mounted on the probe such that, when inserted inside the spectrometer magnet, the channel axis (the long axis of the needle morphology) was perpendicular to \vec{B}_0 and parallel to the rotation axis of the goniometer probe.

III. SYMMETRY PROPERTIES

A. Results

1. Differential scanning calorimetry

On cooling cyclohexane/thiourea from ambient temperature, differential scanning calorimetry (Fig. 2) indicates exo-

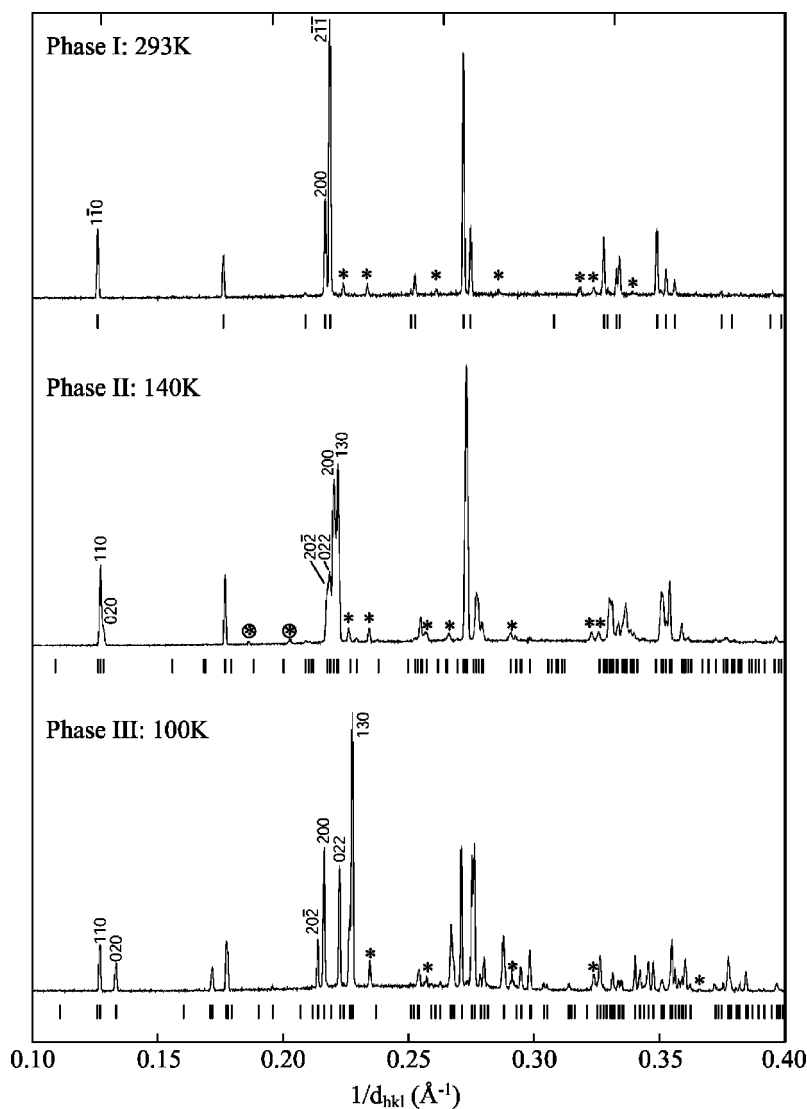


FIG. 3. Synchrotron x-ray powder diffraction patterns recorded for the cyclohexane/thiourea inclusion compound in phase I at 293 K, in phase II at 140 K, and in phase III at 100 K. The peaks marked with asterisks are due to pure thiourea and those marked with circled asterisks are due to pure cyclohexane. The calculated reflection positions for the inclusion compound are marked under each diffraction pattern.

therms (peak-maximum temperatures) at 148 and 127 K. These temperatures identify the three phases, in agreement with previous literature,¹⁸ denoted phase I (above T_{c1} = 148 K), phase II (between T_{c1} and T_{c2} = 127 K), and phase III (below T_{c2}). On subsequently warming the same sample of cyclohexane/thiourea, endotherms are observed (Fig. 2) at 130 and 149 K. Clearly, there is thermal hysteresis in the transition occurring at T_{c2} , corroborated by the observation of the coexistence of phases II and III by ²H NMR over a temperature range of approximately 3–4 K around T_{c2} (see Sec. IV). In addition, we note that for cyclohexane-*d*₁₂/thiourea and cyclohexane/thiourea-*d*₄, the transition from phase II to phase III is observed at values of T_{c2} that are 3 K higher than that observed for a sample of the cyclohexane/thiourea inclusion compound with natural isotopic abundances.

2. Powder x-ray diffraction

The experimental synchrotron x-ray powder diffraction patterns are shown in Fig. 3 in the region $0.1 \text{ \AA}^{-1} \leq 1/d_{hkl} \leq 0.4 \text{ \AA}^{-1}$. Small amounts of pure thiourea and pure cyclo-

hexane may be produced during the grinding of the sample and under exposure to x-ray radiation.¹⁹ Thus low intensity peaks assigned to pure thiourea (indicated by stars on Fig. 3) can be indexed on the basis of the orthorhombic lattice of pure thiourea^{20,21} with space group $Pnma$ at 293 K and space group $P2_1ma$ at 140 and 100 K. Other very low intensity peaks assigned to pure cyclohexane (indicated by circled asterisks on Fig. 3) have been indexed on the basis of the $C2/c$ space group²² at 140 K. No reflections due to pure cyclohexane were observed at 100 K (a fresh sample was used at this temperature). The powder diffraction pattern of the cyclohexane/thiourea inclusion compound recorded at 295 K can be indexed by a lattice with rhombohedral metric symmetry, with $a = 10.0405(3) \text{ \AA}$ and $\beta = 104.095(1)^\circ$. Systematic absences are consistent with space group $R\bar{3}c$, as determined previously from single crystal x-ray diffraction data.¹⁰

On passing below the phase transition temperature T_{c1} , splitting of the peaks assigned to the cyclohexane/thiourea inclusion compound is observed together with the appearance of some new peaks (Fig. 3). For example, the peaks indexed as $(1\bar{1}0)$, (200) , and $(2\bar{1}\bar{1})$ in phase I each split into two peaks in phase II (see Fig. 3 middle). The powder dif-

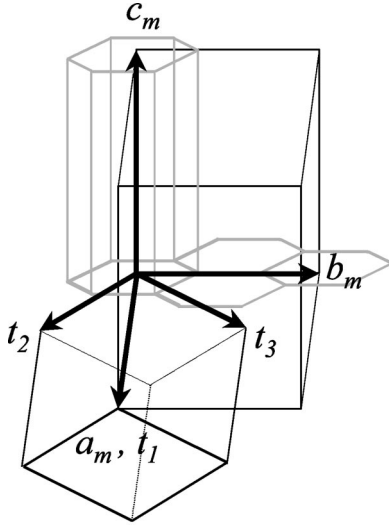


FIG. 4. Schematic representation of the monoclinic lattice ($\vec{a}_m, \vec{b}_m, \vec{c}_m$) with respect to the primitive rhombohedral lattice ($\vec{t}_1, \vec{t}_2, \vec{t}_3$) of phase I used to describe the temperature dependence of the lattice parameters in all three phases.

fraction pattern is indexed by a lattice with monoclinic metric symmetry with the following lattice parameters at 140 K: $a = 9.9876(2)$ Å, $b = 15.5509(3)$ Å, $c = 12.4295(3)$ Å, and $\beta = 114.640(1)^\circ$. All peaks except those marked by asterisks (pure thiourea) or circled asterisks in Fig. 3 (middle) are indexed on the basis of this lattice. Furthermore, from the systematic absences of reflections in the powder diffraction pattern recorded at 140 K, phase II is assigned unambiguously to space group $P12_1/a1$.

In phase III, the number of reflections due to the inclusion compound is the same as for phase II, as shown in Fig. 3 (bottom). It is clear that the phase transition occurring at T_{c2} is associated with an abrupt change of the lattice parameters, but with no other changes evident between phases II and III. At 100 K, the powder diffraction pattern of the inclusion compound is indexed by a monoclinic lattice, with lattice parameters $a = 10.2111(6)$ Å, $b = 14.9745(3)$ Å, $c = 12.4059(2)$ Å, and $\beta = 115.1722(9)^\circ$. As in phase II, the conditions for systematic absences indicate that the space group is $P12_1/a1$.

In order to follow the lattice distortion in the three phases, we require to adopt a common set of lattice parameters. Let \vec{t}_1 , \vec{t}_2 , and \vec{t}_3 be the basic vectors of the primitive rhombohedral lattice in phase I. Then, the basic vectors \vec{a}_m , \vec{b}_m , and \vec{c}_m of the monoclinic lattice (phases II and III) are given by⁹

$$\begin{aligned}\vec{a}_m &= \vec{t}_1, \\ \vec{b}_m &= -\vec{t}_2 + \vec{t}_3, \\ \vec{c}_m &= -\vec{t}_1 - \vec{t}_2 - \vec{t}_3,\end{aligned}\quad (1)$$

where \vec{c}_m is parallel to the (threefold) channel axis and \vec{b}_m is perpendicular to this axis (Fig. 4). Using the powder x-ray diffraction patterns recorded on the laboratory diffracto-

meter, we have indexed the three phases on the basis of a monoclinic unit cell, using Eq. (1) for phase I, and Fig. 5 shows the temperature dependence between 30 and 300 K of the parameters a_m , b_m , c_m and the monoclinic angle β_m . As shown in Fig. 5, c_m remains essentially constant in all three phases. In phase I, a_m and b_m decrease slightly on cooling, whereas β_m increases. However a_m , b_m , c_m , and β_m are not independent lattice parameters in the undistorted rhombohedral phase I, as

$$\begin{aligned}\cos\left(\beta_m - \frac{\pi}{2}\right) &= \frac{b_m}{\sqrt{3}a_m}, \\ \sin\left(\beta_m - \frac{\pi}{2}\right) &= \frac{c_m}{3a_m}.\end{aligned}\quad (2)$$

It turns out that the temperature dependence of a_m , b_m , and β_m in phase I is related to the thermal contraction of the host structure in the plane perpendicular to \vec{c}_m . On lowering the temperature below T_{c1} , there is clearly a marked change in the temperature dependences of a_m , b_m , and β_m , whereas c_m still follows the same type of behavior as in phase I. Thus, on passing below T_{c1} , the monoclinic unit cell begins to distort from the parent rhombohedral cell and on lowering the temperature down to T_{c2} , this distortion evolves continuously. At T_{c2} , there are abrupt changes in the lattice parameters a_m , b_m , and β_m , but not in c_m . On cooling below T_{c2} (phase III), the lattice parameters do not change significantly, and the small changes observed within phase III may be attributed to the effects of thermal contraction. Indeed, extrapolations of the variations of the lattice parameters in phase I, due to the thermal contraction, have essentially the same slopes as those observed in phase III (Fig. 5).

In summary, the high-temperature phase I is rhombohedral with space group $R\bar{3}c$ and the primitive rhombohedral unit cell contains $Z=2$ formula units, i.e., two cyclohexane molecules and six thiourea molecules. Phase II is monoclinic, with space group $P12_1/a1$ ($Z=4$). We note that this is a favorable case in which space group assignment can be made uniquely from systematic absences. It is important to note that space group $P12_1/a1$ is a subgroup of $R\bar{3}c$.²³ The thermal evolution of the lattice parameters from phase I to phase II is continuous in character at the transition temperature T_{c1} , so that the transition from phase I to phase II exhibits all the characteristics of a second order phase transition. On passing below T_{c2} , another monoclinic phase (phase III) is produced, with the same space group as phase II, and again $Z=4$ (isostructural phase transition). The abrupt changes in the lattice parameters and the strong thermal anomaly occurring at T_{c2} are characteristic of a first order phase transition. Finally, we emphasize that from previously published single crystal x-ray diffraction experiments,⁹ it was concluded that the phase transition between phases II and III does not involve any change in the crystal symmetry

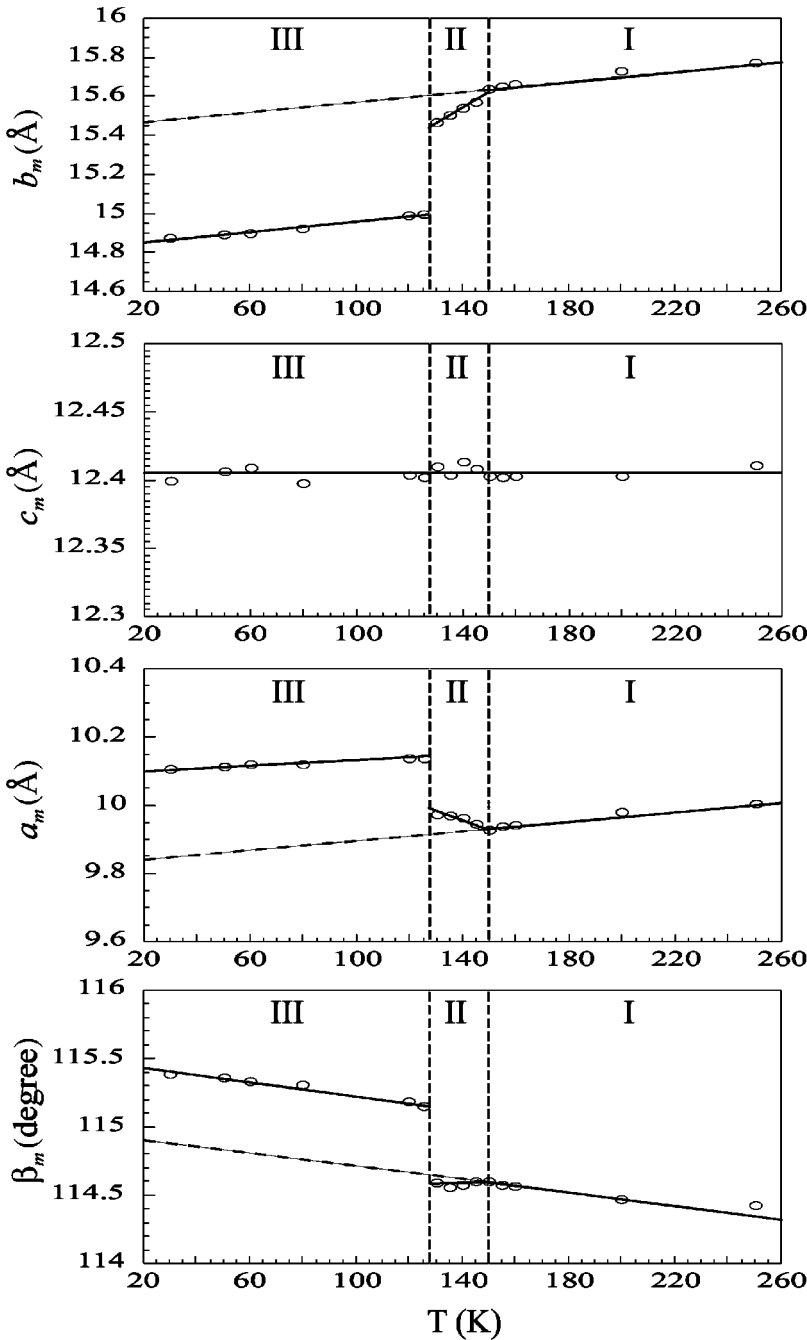


FIG. 5. Temperature dependence of the parameters a_m , b_m , c_m , and β_m of the monoclinic unit cell in the cyclohexane/thiourea inclusion compound. The vertical lines represent the phase transition temperatures. In phase I, the rhombohedral structure is referred to a monoclinic unit cell using Eq. (1). Note that the slope describing the temperature dependence of each lattice parameter in phase I is extrapolated to phase III in order to compare the thermal expansion in these two phases. The estimated error bars lie within the size of the symbols.

and that in both monoclinic phases there is no glide plane along \vec{c}_m , in agreement with the conclusions reached in the present work.

B. Discussion

From the knowledge of space groups and lattice parameters of all structural phases of the cyclohexane/thiourea inclusion compound, together with the fact that the $I \rightleftharpoons II$ and the $II \rightleftharpoons III$ transitions have been established to be of second order and first order, respectively, it is of importance to describe the phase transitions in terms of order parameters defined on the basis of the symmetry principles of Landau theory.

1. Group theory

From Eq. (1) we determine that the transition from phases I to II is driven by a lattice instability occurring at point $F(0\frac{1}{2}\frac{1}{2})$ of the rhombohedral Brillouin zone, i.e., at the zone boundary point in phase I, which is replaced at the zone center in phase II. We note that the monoclinic unit cell defined in Eq. (1) is not the only possible cell belonging to the $P12_1/a1$ setting that may be derived from the rhombohedral phase. Indeed, two other equivalent cells deduced from Eq. (1) by rotations of $\pm 2\pi/3$ around the threefold rhombohedral axis can be found, with the following basic vectors:

$$\begin{aligned}\vec{a}'_m &= \vec{t}_2, \\ \vec{b}'_m &= -\vec{t}_1 + \vec{t}_3, \\ \vec{c}'_m &= -\vec{t}_1 - \vec{t}_2 - \vec{t}_3,\end{aligned}\quad (3)$$

$$\begin{aligned}\vec{a}''_m &= \vec{t}_3, \\ \vec{b}''_m &= -\vec{t}_1 + \vec{t}_2, \\ \vec{c}''_m &= -\vec{t}_1 - \vec{t}_2 - \vec{t}_3.\end{aligned}\quad (4)$$

In these cases, points $F'(\frac{1}{2}0\frac{1}{2})$ and $F''(\frac{1}{2}\frac{1}{2}0)$ become zone center points of the monoclinic lattices Eqs. (3) and (4), respectively. The three sets of basic vectors defined in Eqs. (1), (3), and (4) correspond to the three energetically equivalent ferroelastic domains that exist in the low-temperature phases II and III, as shown by single-crystal ^2H NMR experiments (see Sec. IV below).

The wave-vector group at point F is C_{2h} so that there are three arms in the star of this wave vector, namely, points F , F' , and F'' . It follows that all space group representations at point F , denoted as F_1^+ , F_2^+ , F_1^- , and F_2^- are three dimensional.^{23,24} From classical group theoretical considerations, we determine that F_1^+ induces the $P12/c1$ space group, F_2^+ induces $P12_1/a1$, F_1^- induces $P12/a1$ and F_2^- induces $P12_1/c1$ with lattice parameters as defined in Eq. (1). So, the transition $\text{I} \Rightarrow \text{II}$ is unambiguously induced by a three-dimensional order parameter belonging to the F_2^+ irreducible representation.²³ Let us call ζ_1 , ζ_2 , and ζ_3 the three components of this order parameter that are associated with points F , F' , and F'' , respectively. Hence, we assign the ferroelastic states described in Eqs. (1), (3), and (4) for the monoclinic phases to the three equivalent solutions $\zeta_i \neq 0$, $\zeta_{i \neq j} = 0$, with $i, j = 1, 2$, and 3 .

The F_2^+ representation fulfills both Landau and Lifshitz criteria^{23,25} allowing a second-order transition to take place between the commensurate phases I and II. In contrast, the isostructural transition between phases II and III, induced by the identity representation of phase II, is necessarily of first order. These conclusions are in full agreement with all experimental data.

In phase I, the six thiourea molecules occupying sites with C_2 symmetry constitute one family, and the two cyclohexane molecules occupying sites with D_3 symmetry also constitute one family.¹⁰ Following the group to subgroup relation existing between phase I and phases II and III, it is easy to deduce that in both phases II and III, thiourea molecules are in general positions (sites C_1) and thus constitute three distinct families and that cyclohexane molecules, which also occupy C_1 sites, constitute one family.

2. Landau theory and lattice distortion

The image of the order parameter belonging to the F_2^+ representation is O , so that the Landau free-energy expansion is written as^{23,25}

$$\begin{aligned}\Delta\Phi(\zeta) &= \frac{1}{2}A(T)(\zeta_1^2 + \zeta_2^2 + \zeta_3^2) + \frac{1}{4}B(\zeta_1^2 + \zeta_2^2 + \zeta_3^2)^2 \\ &+ \frac{1}{4}C(\zeta_1^4 + \zeta_2^4 + \zeta_3^4) + \dots,\end{aligned}\quad (5)$$

where the coefficient $A(T) = a(T - T_{c1})$ with $a > 0$ changes sign at the transition temperature T_{c1} . When truncated to the fourth order, $\Delta\Phi(\zeta)$ admits only two low-temperature phases ($T < T_{c1}$) associated with the equilibrium values

$$\begin{aligned}\text{phase II: } \zeta &= \zeta_1 \neq 0, \zeta_2 = \zeta_3 = 0 \\ (\text{space group } P12_1/a1, Z=4),\end{aligned}\quad (6)$$

$$\begin{aligned}\text{phase II': } \zeta_1 &= \zeta_2 = \zeta_3 = \frac{1}{\sqrt{3}}\zeta \neq 0 \\ (\text{space group } R\bar{3}, Z=8).\end{aligned}\quad (7)$$

The monoclinic phase of interest in this study is stable for values of the coefficients B and C such as $B > 0$ and $B + C > 0$, whereas the possible rhombohedral low temperature phase $R\bar{3}$ would be stable for $3B + C > 0$ and $C > 0$. The first order transition line between phases II and II' corresponds to $C = 0$.

The elastic energy¹¹ is

$$\Delta\Phi(e) = \frac{1}{2} \sum_{i,j=1}^6 c_{ij}^0 e_i e_j, \quad (8)$$

where the c_{ij}^0 are the ‘‘bare’’ elastic constants and the e_i are the strain tensor components (Voigt notation). Usually, in rhombohedral crystals with class $\bar{3}m$, the C_2 symmetry axis is set parallel to the x direction.²⁶ In the following discussion, we take this symmetry axis parallel to the y direction (\vec{b}_m), in order to keep the same setting in both phases I ($R\bar{3}c$) and II [$P12_1/a1$, see Eq. (1)]. Under these conditions, the independent nonzero values of c_{ij}^0 entering into Eq. (8) are of the form

$$\begin{pmatrix} c_{11}^0 & c_{12}^0 & c_{13}^0 & 0 & c_{15}^0 & 0 \\ c_{12}^0 & c_{11}^0 & c_{13}^0 & 0 & -c_{15}^0 & 0 \\ c_{13}^0 & c_{13}^0 & c_{33}^0 & 0 & 0 & 0 \\ 0 & 0 & 0 & c_{44}^0 & 0 & -c_{15}^0 \\ c_{15}^0 & -c_{15}^0 & 0 & 0 & c_{44}^0 & 0 \\ 0 & 0 & 0 & -c_{15}^0 & 0 & \frac{1}{2}(c_{11}^0 - c_{12}^0) \end{pmatrix}.$$

The decomposition of the symmetrized square of the order parameter representation F_2^+ into irreducible space-group representations gives

$$[F_2^+]^2 = A_{1g} \oplus E_g \oplus F_1^+ \quad (9)$$

and the direct product $E_g \otimes E_g$ gives $A_{1g} \oplus A_{2g} \oplus E_g$. It follows that quadratic-linear coupling terms between order parameter components and strain components with $A_{1g} [(e_1 + e_2), e_3]$ and $E_g [(e_1 - e_2), e_4, e_5, e_6]$ symmetry can be included as invariants in the free-energy expansion

$$\begin{aligned} \Delta\Phi(\zeta, e) = & D\{(2\zeta_1^2 - \zeta_2^2 - \zeta_3^2)[(e_1 - e_2) + e_5] \\ & - \sqrt{3}(\zeta_2^2 - \zeta_3^2)(e_4 + e_6)\} + E(\zeta_1^2 + \zeta_2^2 + \zeta_3^2) \\ & \times (e_1 + e_2) + F(\zeta_1^2 + \zeta_2^2 + \zeta_3^2)e_3. \end{aligned} \quad (10)$$

Thus, the thermodynamic potential used to describe the transition from phase I to phase II in the cyclohexane/thiourea inclusion compound is

$$\Delta\Phi = \Delta\Phi(\zeta) + \Delta\Phi(e) + \Delta\Phi(\zeta, e). \quad (11)$$

The minimization equations $\partial\Delta\Phi/\partial e_i = 0$, together with Eq. (6), give expressions for the variation of strain components as a function of the order parameter in the monoclinic phase II:

$$\begin{aligned} e_1 + e_2 &= \frac{2Fc_{13}^0 - 2Ec_{33}^0}{(c_{11}^0 + c_{12}^0)c_{33}^0 - 2(c_{13}^0)^2} \zeta^2, \\ e_3 &= \frac{2Ec_{13}^0 - F(c_{11}^0 + c_{12}^0)}{(c_{11}^0 + c_{12}^0)c_{33}^0 - 2(c_{13}^0)^2} \zeta^2, \\ e_1 - e_2 &= \frac{2D(2c_{15}^0 - c_{44}^0)}{(c_{11}^0 - c_{12}^0)c_{44}^0 - 2(c_{15}^0)^2} \zeta^2, \\ e_5 &= \frac{2D[c_{15}^0 - (c_{11}^0 - c_{12}^0)]}{(c_{11}^0 - c_{12}^0)c_{44}^0 - 2(c_{15}^0)^2} \zeta^2, \\ e_4 = e_6 &= 0. \end{aligned} \quad (12)$$

Here we find a classical result for an improper ferroelastic transition,^{11,25} showing that both volume strain components e_1, e_2 , and e_3 and spontaneous strain $(e_1 - e_2)$ and e_5 vary as the square of the order parameter ζ . In other words, $(e_1 - e_2)$ and e_5 are secondary order parameters. Putting Eq. (12) back into Eq. (11) provides the “effective” potential for phase II:

$$\Delta\tilde{\Phi} = \frac{1}{2}a(T - T_{c1})\zeta^2 + \frac{1}{4}(B + C + \Gamma)\zeta^4 + \dots, \quad (13)$$

where Γ is a constant that depends on the values of the Landau expansion coefficients D, E, F and on the “bare” elastic constants. Then, the equilibrium value of the order parameter is

$$\zeta^2 = \frac{a(T_{c1} - T)}{B + C + \Gamma} \quad (14)$$

so that a linear temperature dependence is expected for the strain tensor components given in Eq. (12). The stability condition is now $B' = B + C + \Gamma > 0$.

In order to account for the isostructural phase transition that occurs at T_{c2} , we may introduce in Eq. (5) the sixth

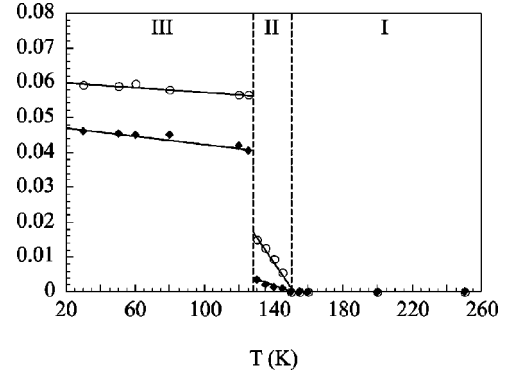


FIG. 6. Temperature dependence of the spontaneous strain components $e_1 - e_2$ (open circles) and e_5 (filled diamonds) which describe the distortion of the unit cell in the cyclohexane/thiourea inclusion compound. The vertical lines represent the phase transition temperatures between phases I, II, and III. The estimated error bars lie within the size of the symbols.

and eighth order invariants. Since Eq. (12) is still valid, the “effective” potential in the monoclinic subspace ($\zeta = \zeta_1 \neq 0, \zeta_2 = \zeta_3 = 0$) becomes

$$\Delta\tilde{\Phi} = \frac{1}{2}a(T - T_{c1})\zeta^2 + \frac{1}{4}B'\zeta^4 + \frac{1}{6}G\zeta^6 + \frac{1}{8}H\zeta^8. \quad (15)$$

The possible phase diagrams related to such a potential have already been studied in detail.^{25,27-29} It turns out that for appropriate values of the coefficients $B' > 0, G < 0$, and $H > 0$, the potential $\Delta\tilde{\Phi}$ is able to reproduce the observed phase transition sequence I ($R\bar{3}c$) \rightleftharpoons II ($P12_1/a1$) \rightleftharpoons III ($P12_1/a1$), where the transition at T_{c1} from phase I to phase II is of second order and the transition at $T_{c2} < T_{c1}$ from phase II to phase III is of first order. According to the ζ^8 model [Eq. (15)], the simple linear temperature dependence of ζ^2 [Eq. (14)] is no longer expected. Instead, in phase II close to T_{c1} , a variation such as $\zeta \propto (T_{c1} - T)^\beta$ with $\beta < 1/2$ should be observed, because of the nearness of a critical point in the corresponding phase diagram.^{25,28,29} Then, a jump in the equilibrium value of ζ occurs at T_{c2} and ζ continues to increase in phase III as temperature is decreased.^{28,29}

Obviously, Eq. (2) does not apply in the monoclinic distorted phases, so that deviations from Eq. (2) are a measure of the spontaneous strains. Hence, the shear distortions $e_{xx} - e_{yy} = e_1 - e_2$ and $2e_{xz} = e_5$ are given by

$$\begin{aligned} e_1 - e_2 &= 1 - \frac{b_m}{\sqrt{3}a_m \cos(\beta_m - \pi/2)}, \\ e_5 &= 1 - \frac{c_m}{3a_m \sin(\beta_m - \pi/2)}. \end{aligned} \quad (16)$$

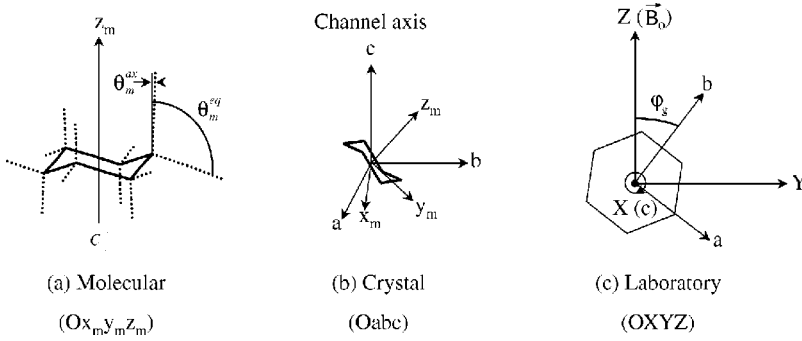


FIG. 7. (a) The chair conformation of cyclohexane, (b) representation of the crystal frame ($Oabc$) and molecular frame ($Ox_my_mz_m$) within the thiourea inclusion compound, and (c) representation of the geometry of the single crystal ^2H NMR experiment within the laboratory axis system ($OXYZ$) (where the magnetic field \vec{B}_0 lies along the Z axis by convention). In (c), the reference axis \vec{b} is perpendicular to a face of the single crystal morphology.

The observed temperature dependences of $(e_1 - e_2)$ and e_5 through the sequence of phases of the cyclohexane/thiourea inclusion compound are reported in Fig. 6. Both strain components increase smoothly on crossing T_{c1} , as expected for a second order phase transition. Furthermore, in the limit of experimental accuracy, $(e_1 - e_2)$ and e_5 exhibit the linear temperature dependence of Eq. (14) derived from the ζ^4 model [Eq. (13)]. Thus, there is no need to introduce the ζ^6 and ζ^8 terms in the Landau free energy expansion. At T_{c2} , abrupt jumps occur in $(e_1 - e_2)$ and e_5 , associated with a much stronger lattice distortion. Indeed, at T_{c2} , $(e_1 - e_2)$ and e_5 approach four times and ten times their respective highest values in phase II (just above T_{c2}). Then, on decreasing temperature within phase III, the strain components increase only by 2% between T_{c2} and 30 K. These very small variations of $(e_1 - e_2)$ and e_5 in phase III, together with the huge discontinuities observed at T_{c2} , indicate that the production of phase III is not governed by the order parameter ζ that induces the second order transition from phase I to phase II. Rather than referring to the complex ζ^8 model, we merely assign the temperature dependence of spontaneous strain components within phase III to the thermal contraction of the host lattice.

IV. MOLECULAR DYNAMICS

A. Theoretical background

In ^2H NMR of diamagnetic organic solids the dominant nuclear spin interaction is usually the interaction of the electric quadrupole moment of the ^2H nucleus with the electric field gradient at the position of the nucleus. This interaction (the quadrupolar interaction) can be characterized by the quadrupole coupling tensor Q . In its principal axis system, the principal components of this traceless tensor are taken such that $|Q_{zz}| \geq |Q_{yy}| \geq |Q_{xx}|$. The quadrupole interaction is usually defined in terms of two parameters: the quadrupole coupling constant $\chi = Q_{zz}$ and the asymmetry parameter $\eta = (|Q_{yy}| - |Q_{xx}|) / |Q_{zz}|$. In the case of a CD_2 group, it is usually a valid approximation to assume that the z axis of the Q^P tensor (where the superscript P refers to the principal axis system) is collinear with the C–D bond and that Q^P has axial symmetry (thus $\eta = 0$).

In the analysis of ^2H NMR line shapes, three distinct dynamic regimes can be identified. When the rate (κ) of motion is in the slow motion regime, $\kappa \leq 10^3 \text{ s}^{-1}$, the ^2H NMR spectrum is insensitive to the occurrence of the mo-

tion. In the intermediate motion regime, $10^3 \leq \kappa \leq 10^7 \text{ s}^{-1}$, the ^2H NMR spectrum depends critically on the mechanism and rate of the molecular motion. In the fast motion regime, $\kappa \geq 10^7 \text{ s}^{-1}$, the actual rate of motion cannot be established from analysis of the ^2H NMR spectrum, although information on the geometry and mechanism of the motion can still be obtained.

We note that the comparison of spectra recorded with different echo delays τ_1 provides information concerning the time scale of the dynamic process. Indeed, in a quadrupole echo experiment, if the motion is in the intermediate regime, the line shape can depend significantly on τ_1 .¹⁷ Thus, if the experimental spectrum is found to be independent of τ_1 , it suggests that the dynamic processes are either in the fast motion regime or the slow motion regime.

We now define the molecular axis system ($Ox_my_mz_m$) shown in Fig. 7(a), where the z_m axis is collinear with the C_3 symmetry axis (denoted hereafter C_3^m) of the cyclohexane molecule [Fig. 7(a)], the crystal axis system ($Oabc$), where the c axis is collinear with the channel axis [Fig. 7(b)], and the laboratory axis system ($OXYZ$), where the Z axis is the direction of the applied magnetic field \vec{B}_0 [Fig. 7(c)]. In the fast motion regime, the averaged components of the quadrupole coupling tensor in the crystal axis system (labeled C) can be obtained by taking a weighted average over all orientations $i = 1, \dots, N$ of the tensor (i.e., all orientations of the C–D bond) sampled during the motion^{30,31}

$$\bar{Q}^C = \sum_{i=1}^N p_i \bar{Q}_i^C, \quad (17)$$

where p_i denotes the probability of orientation i given by the polar angles (θ_i^c, ϕ_i^c) . For a given orientation of \bar{Q}^C [Eq. (17)] in the laboratory axis system, the ^2H NMR spectrum comprises two lines separated by frequency $\Delta\nu$:

$$\Delta\nu = \frac{3}{2} \bar{\chi} \left[P_2(\cos \theta) + \frac{\bar{\eta}}{2} \sin^2 \theta \cos 2\phi \right], \quad (18)$$

where (θ, ϕ) are the polar angles for the orientation of the crystal in the laboratory frame, $P_2(\cos \theta)$ is the second Legendre polynomial $(3 \cos^2 \theta - 1)/2$, \bar{Q}_{xx} , \bar{Q}_{yy} , and \bar{Q}_{zz} are the components of \bar{Q}^C in the motionally averaged principal axis system, $\bar{\chi} = \bar{Q}_{zz}$ is the motionally averaged quadrupole coupling constant and $\bar{\eta} = (|\bar{Q}_{yy}| - |\bar{Q}_{xx}|) / |\bar{Q}_{zz}|$ is the motionally averaged asymmetry parameter.

B. Microscopic model of the dynamics of the guest molecules

Our aim is now to elaborate a multidimensional pseudospin model^{32–34} of the dynamic properties of the guest molecules in the cyclohexane/thiourea inclusion compound on the basis of the symmetry rules imposed by the crystal structure. At first, we note that a detailed low frequency Raman scattering study has been carried out recently on a single crystal of cyclohexane/thiourea, through the sequence of phases.³⁵ No soft mode could be observed, thus showing that there is no detectable displacive contribution in the mechanisms of the phase transitions. Thus, it can be stated safely that the transition from phase I to phase II is essentially of order-disorder type. We now describe the models that will be used to describe the dynamics of the guest molecules in the three structural phases of the inclusion compound. These models will be applied to our ²H NMR results in order to understand the evolution of the dynamic behavior as a function of temperature.

As discussed below, the dynamics of the guest molecules in cyclohexane/thiourea can be described in terms of three dynamic processes:^{14,15,35–37} (1) ring inversion, which does not occur on the ²H NMR time scale below about 220 K, (2) reorientation of the cyclohexane molecule about its C_3^m axis (effective in all phases I, II, and III), and (3) reorientation of the C_3^m axis with respect to the host channel (effective in phases I and II). Throughout the temperature range (127–297 K) covered in the present study, processes (2) and (3) are in the fast motion regime ($\kappa \geq 10^7 \text{ s}^{-1}$). In addition, in the cyclohexane molecule, two types of deuterons must be distinguished, i.e., axial deuterons with polar angle $\theta_m^a = 2.6^\circ$ in the molecular axis system [Fig. 7(a)] and equatorial deuterons with $\theta_m^e = 109.7^\circ$.^{38,39} Assuming an N -site $2\pi/N$ jump model with $N \geq 3$ for fast reorientation of the cyclohexane molecule about its C_3^m axis, the motionally averaged quadrupole coupling tensor is axially symmetric (i.e., $\bar{\eta} = 0$) and the motionally averaged quadrupole coupling constant (denoted hereafter $\bar{\chi}_{C_3^m}^j$) for this motion is

$$\bar{\chi}_{C_3^m}^j = \chi |P_2(\cos \theta_m^j)|, \quad (19)$$

where we use the notation $j = a$ for axial deuterons and $j = e$ for equatorial deuterons. Thus, for this motion, the ²H NMR spectrum will comprise two pairs of resonance lines, one pair of lines separated by frequency $\Delta\nu^a$ for axial deuterons and the other pair of lines separated by frequency $\Delta\nu^e$ for equatorial deuterons. The ratio of the quadrupole splittings for the axial deuterons ($\Delta\nu^a$) and equatorial deuterons ($\Delta\nu^e$) is

$$\frac{\Delta\nu^a}{\Delta\nu^e} \approx 3. \quad (20)$$

If, in addition to the rapid reorientation about the C_3^m axis of the cyclohexane molecule, there is anisotropic motion of the

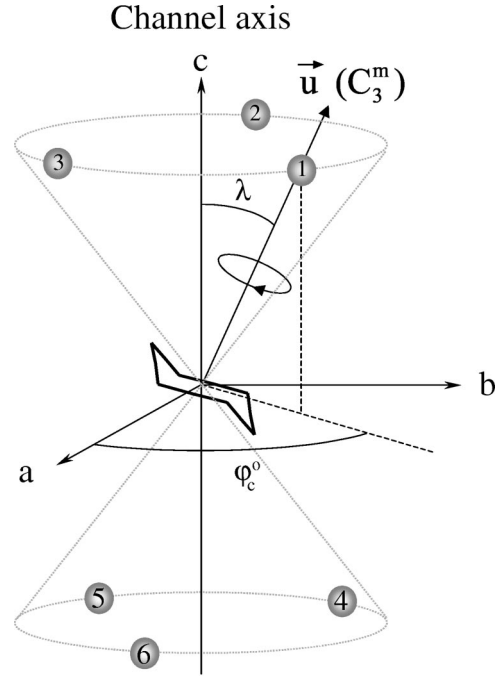


FIG. 8. Representation of the six orientations of the molecular C_3^m axis with respect to the crystal frame ($Oabc$). The orientations labeled 1, 2, and 3 are denoted the “up” sites, and the orientations labeled 4, 5, and 6 are denoted the “down” sites. The orientation labeled 1 is described by the polar angles (λ, φ_c^0) . The orientations labeled 2 to 6 are deduced by the symmetry operations of the D_3 point group.

C_3^m axis itself, the values of the splittings $\Delta\nu^a$ and $\Delta\nu^e$ will be modified but the ratio $\Delta\nu^a/\Delta\nu^e$ will remain constant.

According to x-ray diffraction data,¹⁰ the guest molecules at room temperature are in instantaneous general positions and the site symmetry is D_3 . Considering the symmetry operations of the D_3 point group, the reorientational dynamics of the C_3^m axis of each cyclohexane molecule in the inclusion compound may be described by means of the following jump model. We define the orientation of the guest molecule in the unit cell by a unit vector \vec{u} collinear with the C_3^m axis, with orientation defined by the angles (θ_c, φ_c) with respect to the crystal frame. The C_3^m axis jumps rapidly between six orientations ($i = 1, \dots, 6$) generated by the six symmetry operations of the D_3 point group (see Fig. 8). The orientations i have occupation probabilities $p_i = \frac{1}{6}$, and polar angles

$$\theta_c^i = \lambda, \quad \varphi_c^i = \varphi_c^0 + \frac{2\pi(i-1)}{3} \quad \text{for } i = 1, 2, 3,$$

$$\theta_c^i = \pi - \lambda, \quad \varphi_c^i = \pi - \varphi_c^0 + \frac{2\pi(i-4)}{3} \quad \text{for } i = 4, 5, 6,$$

where λ is the “tilt” angle between the C_3^m axis and the channel axis \vec{c} . Taking into account the fast reorientation of the cyclohexane molecule about its C_3^m axis [Eq. (19)], the motionally averaged quadrupole coupling constant in Eq. (18) becomes

$$\bar{\chi}^j = \bar{\chi}_{C_3^m}^j |P_2(\cos \lambda)| \quad (21)$$

and the motionally averaged asymmetry parameter is $\bar{\eta} = 0$. From analysis of molecular dynamics simulations of cyclohexane/thiourea carried out at 273 K in phase I³⁶ it was found that $\lambda \approx 60^\circ$ and $\varphi_c^0 \approx 60^\circ$.

As the transition between phases I and II is of second order, the six orientations of the molecular C_3^m axis discussed for phase I are maintained in phase II. Several dynamic models could be proposed in which the angles between sites and/or the occupation probabilities are allowed to deviate from those observed in phase I. However, as phase II is characterized by a weak distortion from the structure of phase I, with the angles of the thiourea channels varying only weakly from the hexagonal values, it is reasonable to assume that the loss of the C_3 symmetry axis on crossing the phase transition temperature is due to a continuous change of the occupation probabilities in each orientation rather than a substantial change in the orientations themselves. We denote the occupation probability of the guest molecule in orientation i as p_i , with $\sum_{i=1}^6 p_i = 1$. In phase II, the C_1 guest site symmetry imposes no constraint that the occupation probabilities

must be equal, and the temperature dependence of the probabilities p_i can be described by means of pseudospin variables. By using the method of projection operators described in the Appendix, we define six pseudospin coordinates s_i , associated with the six symmetry operations of the D_3 point group, as a function of the occupation probabilities p_i . These pseudospin coordinates represent the order parameter components of the system, and s_i can be associated with a component of the motion of the guest molecules. Indeed, the zero value of the first coordinate s_1 does not induce a symmetry breaking at the transition between phases I and II, so that this pseudospin coordinate can be assigned to the rotation of the cyclohexane molecule about its C_3^m axis. The coordinate s_2 describes the ‘‘up-down exchange’’ between opposite orientations labeled as 1, 2, 3 (for ‘‘up’’ orientations) and 4, 5, 6 (for ‘‘down’’ orientations) in Fig. 8. Finally, the degenerate coordinates (s_3, s_4) and (s_5, s_6) are linked to reorientations of the C_3^m axis about the channel axis. By expressing the occupation probabilities as a function of the pseudospin coordinates (see the Appendix) and using Eq. (17), the weighted averaged quadrupole coupling tensor \bar{Q}_{II}^C is

$$\bar{Q}_{\text{II}}^C = -\frac{\chi P_2(\cos \theta_m^j)}{2} \begin{pmatrix} P_2(\cos \lambda) - \frac{9}{4} \sin^2 \lambda (\rho_1 + \rho_2) & \frac{3\sqrt{3}}{4} \sin^2 \lambda (3\rho_2 - \rho_1) & \frac{9}{4} \sin 2\lambda (3\rho_2 - \rho_1) \\ \frac{3\sqrt{3}}{4} \sin^2 \lambda (3\rho_2 - \rho_1) & P_2(\cos \lambda) - \frac{9}{4} \sin^2 \lambda (\rho_1 + \rho_2) & \frac{3\sqrt{3}}{4} \sin^2 \lambda (3\rho_2 - \rho_1) \\ \frac{9}{4} \sin 2\lambda (3\rho_2 - \rho_1) & \frac{3\sqrt{3}}{4} \sin^2 \lambda (3\rho_2 - \rho_1) & -2P_2(\cos \lambda) \end{pmatrix}, \quad (22)$$

where ρ_1 and ρ_2 are linear combinations of s_j ($j=3, \dots, 6$):

$$\begin{aligned} \rho_1 &= \frac{1}{2}(\sqrt{3}s_5 - s_4) = \frac{1}{2}(p_1 - p_3 - p_4 + p_5), \\ \rho_2 &= \frac{1}{2}(\sqrt{3}s_3 - s_6) = \frac{1}{6}(1 - 3p_2 - 3p_6). \end{aligned} \quad (23)$$

The dynamics of the guest molecules are therefore characterized by the tilt angle λ and the two parameters ρ_1 and ρ_2 . It appears from Eqs. (22) and (23) that no information can be obtained on the pseudospin coordinate s_2 (i.e., the ‘‘up-down’’ exchange motion is not probed by the ^2H NMR technique).

Finally, if we refer to literature results,¹⁵ the reorientations of the C_3^m axis with respect to the host structure are frozen in phase III (on the ^2H NMR time scale), so that the motion in this phase can be described simply by means of Eq. (18) with $\bar{\chi}^j = \bar{\chi}_{C_3^m}^j$ and $\bar{\eta} = 0$ (i.e., the only motion effective on the ^2H NMR time scale is reorientation of each cyclohexane guest molecule about its C_3^m axis).

C. Results

We recall [Eq. (1)] that the \vec{c}_m axis is collinear with the channel axis and \vec{b}_m is collinear with the twofold symmetry axis of phase I (and therefore perpendicular to the channel axis). We now define a reference axis \vec{b} perpendicular to a crystal face. In phases II and III, \vec{b} corresponds to the monoclinic axis \vec{b}_m and \vec{a} [see Fig. 7(c)] is the projection of \vec{a}_m on the plane perpendicular to the channel axis. Hereafter, we define φ_g as the angle between the reference axis \vec{b} and the applied magnetic field \vec{B}_0 . In these single crystal ^2H NMR experiments, different crystals were used for some of the temperatures studied and the initial position of the crystal was set as close as practically possible to be with the reference axis \vec{b} parallel to \vec{B}_0 (i.e., with a crystal face perpendicular to \vec{B}_0). Spectra were recorded as a function of reorientation of the single crystal about the channel axis, from the initial φ_g angle (denoted φ_g^0) to $\varphi_g^0 + 180^\circ$ in angular increments $\Delta\varphi_g$.

In phase I, single crystal ^2H NMR spectra were recorded at 163 K as a function of crystal orientation (in steps of $\Delta\varphi_g = 20^\circ$), and as a function of temperature with the crystal

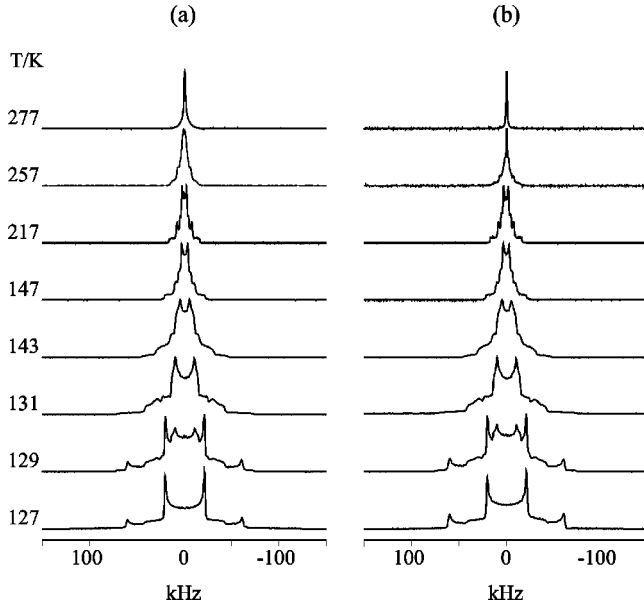


FIG. 9. Experimental ^2H NMR spectra recorded for a powder sample of cyclohexane- d_{12} /thiourea with echo delays of (a) 30 μs and (b) 150 μs . The temperature at which each spectrum was recorded is indicated on the left side.

orientation fixed at φ_g° . In phase II, single crystal ^2H NMR spectra were recorded at 145, 139, and 131 K. In phase III, single crystal ^2H NMR spectra were recorded at 123 and 118 K. At 118 K, spectra were recorded between φ_g° and $\varphi_g^\circ + 180^\circ$ in steps of $\Delta\varphi_g = 3^\circ$. At 145, 139, 131, and 123 K, spectra were recorded between φ_g° and $\varphi_g^\circ + 70^\circ$ in steps of $\Delta\varphi_g = 1^\circ$ and between $\varphi_g^\circ + 70^\circ$ and $\varphi_g^\circ + 180^\circ$ in steps of $\Delta\varphi_g = 10^\circ$.

Figure 9 shows the evolution of the ^2H NMR spectrum for a powder sample of cyclohexane- d_{12} /thiourea as a function of temperature for two different values of the echo delay τ_1 . Between 297 and 217 K, the line shapes are different for the different values of τ_1 , and may be attributed to the occurrence of chair-chair ring inversion of the cyclohexane- d_{12} molecules in the intermediate motion regime¹⁵ (in addition, other reorientational processes occur on a shorter time scale, as discussed below). Below 217 K, the chair-chair ring inversion is not effective on the ^2H NMR time scale and the ^2H NMR line shapes are identical for the two values of echo delay. Thus, all other reorientational processes of the cyclohexane guest molecules occur in the fast motion regime and may be characterized in terms of the motionally averaged quadrupole coupling constant $\bar{\chi}$ and the motionally averaged asymmetry parameter $\bar{\eta}$. Powder ^2H NMR spectra were simulated using the program TURBOPOWDER (Ref. 30) and fitted to the experimental spectra to determine the values of $\bar{\chi}$ and $\bar{\eta}$.

Following previous work,¹⁴ the static quadrupole coupling constant χ for the deuterons in cyclohexane is $\chi = 165$ kHz. Thus, from Eq. (19), we obtain $\bar{\chi}_{C_3^a}^a = 164$ kHz and $\bar{\chi}_{C_3^e}^e = 54$ kHz. In order to follow the temperature dependence of $\bar{\chi}^a$ and $\bar{\chi}^e$, we define the ratio \bar{R} :

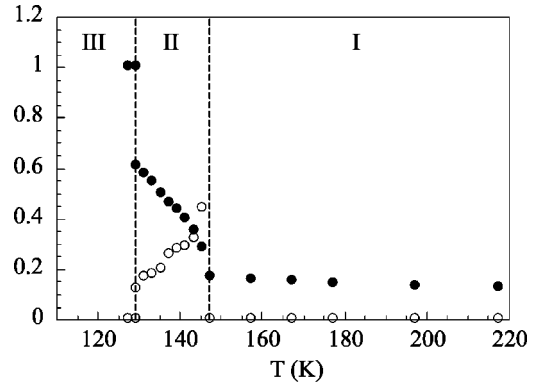


FIG. 10. Variation of the motionally averaged quadrupole coupling constant ratio $\bar{R} = \bar{\chi}^j / \bar{\chi}_{C_3^m}^j$ (filled circles) and the motionally averaged asymmetry parameter $\bar{\eta}$ (open circles) of cyclohexane- d_{12} /thiourea in phases I, II, and III, measured from the powder ^2H NMR spectra.

$$\bar{R} = \frac{\bar{\chi}^a}{\bar{\chi}_{C_3^m}^a} = \frac{\bar{\chi}^e}{\bar{\chi}_{C_3^m}^e}. \quad (24)$$

In Fig. 10, we report the evolution of \bar{R} and $\bar{\eta}$ as a function of temperature in the three structural phases of the inclusion compound.

I. Phase I

As shown in Fig. 10, the motionally averaged quadrupole coupling tensor in phase I is axially symmetric ($\bar{\eta} = 0$). Single crystal ^2H NMR spectra recorded for phase I (between 220 and 150 K) comprise two pairs of peaks (i.e., two quadrupole doublets), with one pair of peaks assigned to the axial deuterons and the other pair of peaks assigned to the equatorial deuterons [Fig. 11(a)]. In each case, the quadrupole splitting $\Delta\nu$ is independent of the crystal rotation angle φ_g , showing that the motionally averaged quadrupole coupling tensors for the axial and equatorial deuterons have axial symmetry, with the principal axes of these tensors aligned along the φ_g rotation axis (channel axis). From the powder ^2H NMR spectra recorded in phase I, the motionally averaged quadrupole splittings corresponding to the magnetic field \vec{B}_0 perpendicular ($\Delta\nu^\perp$) and parallel ($\Delta\nu^\parallel$) to the principal axis of each motionally averaged quadrupole coupling tensor have been measured [see Fig. 11(b)], and these values compare very well with the motionally averaged quadrupole splittings observed from the single crystal ^2H NMR data (Fig. 12). Following the jump model described above and according to Eq. (21), the ratio \bar{R} given in Eq. (24) is theoretically expressed as $|P_2(\cos\lambda)|$. From the experimental values of \bar{R} shown in Fig. 10, we can follow the evolution of the tilt angle λ as a function of temperature in phase I (Fig. 13). Because of the absolute value of the second Legendre polynomial, there are two equivalent mathematical solutions for the tilt angle λ , as shown in Fig. 13. However MD simulations³⁶ have shown that the tilt angle is approximately 60° at 273 K, in very good agreement with one set of

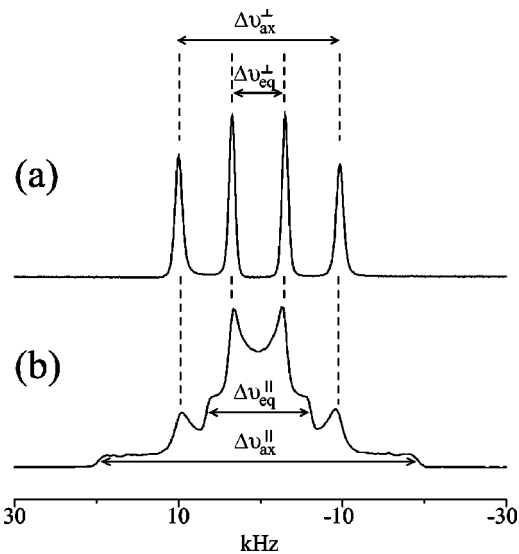


FIG. 11. (a) Experimental single crystal ^2H NMR spectrum recorded with the magnetic field \vec{B}_0 perpendicular to the channel axis, and (b) the corresponding powder ^2H NMR spectrum. Both spectra were recorded for phase I of cyclohexane- d_{12} /thiourea at 167 K with echo delay $30 \mu\text{s}$. The quadrupole splittings corresponding to the orientations with the magnetic field \vec{B}_0 parallel ($\Delta\nu^\parallel$) and perpendicular ($\Delta\nu^\perp$) to the z axis of the motionally averaged quadrupole interaction tensor are indicated.

solutions found from our analysis of the ^2H NMR data (solid line in Fig. 13). Thus, we conclude in favor of the set of solutions for which the tilt angle in phase I is around 60° .

2. Phase II

Between 147 and 129 K, “shoulders” are present on the powder ^2H NMR spectra (Fig. 9) indicating that the motionally averaged quadrupole coupling tensor is no longer axially

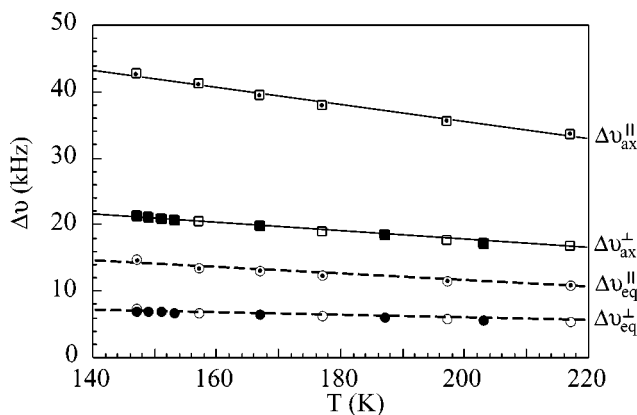


FIG. 12. Plot of the motionally averaged quadrupole splitting $\Delta\nu$ for axial (squares) and equatorial (circles) deuterons of cyclohexane- d_{12} in phase I of cyclohexane- d_{12} /thiourea as a function of temperature. Filled symbols are for the single crystal ^2H NMR experiment with magnetic field \vec{B}_0 perpendicular to the channel axis. Values of $\Delta\nu$ extracted from powder ^2H NMR spectra are indicated by open symbols for the component perpendicular to \vec{B}_0 and by open symbols with a dot for the component parallel to \vec{B}_0 .

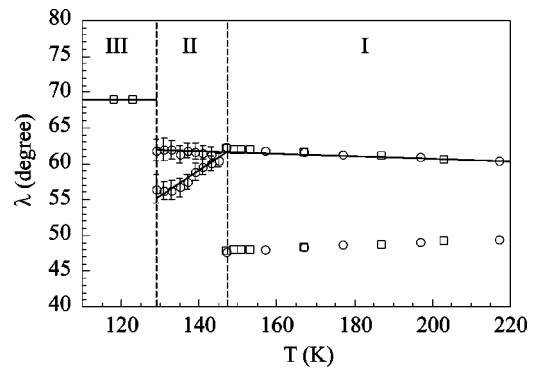


FIG. 13. Variation of the tilt angle λ in phases I, II, and III (separated by the vertical lines) of cyclohexane- d_{12} /thiourea. Circles refer to powder ^2H NMR experiments and squares refer to single crystal ^2H NMR experiments. The error bars in phase II represent the tilt angle solutions that correspond to the experimental values of \bar{R} and $\bar{\eta}$ within an accuracy of 0.1%.

symmetric (i.e., $\bar{\eta} \neq 0$ in phase II, as shown in Fig. 10). Figure 14 shows a stack plot of single crystal ^2H NMR spectra recorded as a function of the crystal rotation angle φ_g for two temperatures in phase II. The evolution of the spectra as a function of rotation angle φ_g can be interpreted in terms of 12 pairs of peaks (quadrupole doublets), of which 6 are assigned to axial deuterons and 6 are assigned to equatorial deuterons. This assignment is facilitated by recalling that, for a given orientation of the cyclohexane molecule, the ratio of

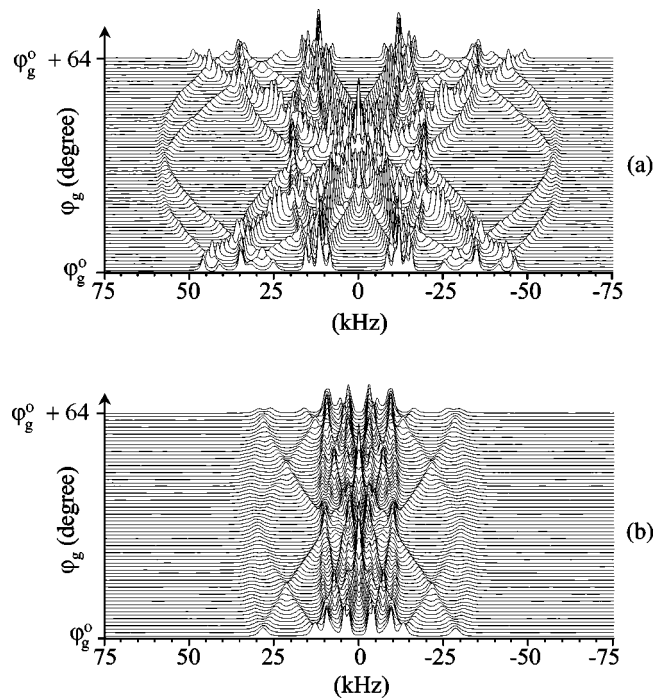


FIG. 14. Experimental single crystal ^2H NMR spectra recorded (with echo delay $30 \mu\text{s}$) for cyclohexane- d_{12} /thiourea in phase II at (a) 131 K and (b) 145 K as a function of rotation (φ_g) about the channel axis, with the channel axis perpendicular to the magnetic field \vec{B}_0 . The plot represents a total variation of 64° in the crystal orientation.

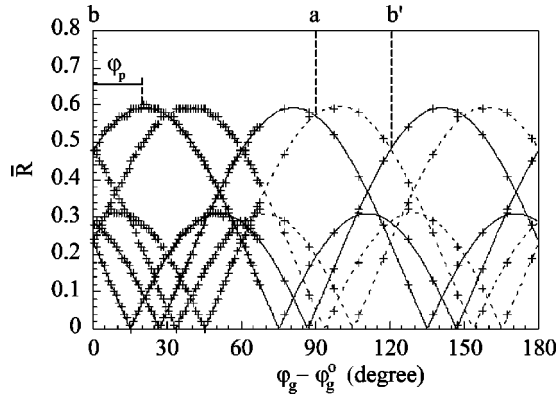


FIG. 15. Plot of $\bar{R}(\varphi_g)$ obtained from single crystal ^2H NMR data recorded (with echo delay $30 \mu\text{s}$) at 139 K in phase II of cyclohexane- d_{12} /thiourea. On the top, the directions of the monoclinic axes are indicated for different twin domains, which differ in orientation by 120° in φ_g .

the quadrupole splittings for the axial and equatorial deuterons is a constant, i.e., $\Delta\nu^a(\varphi_g)/\Delta\nu^e(\varphi_g) \approx 3$. Thus, our results suggest that there are six distinguishable orientations of the motionally averaged quadrupole coupling tensor with respect to the crystal frame, both for axial and equatorial deuterons. Thus, averaged over the dynamic processes, there are six distinguishable orientations of cyclohexane guest molecules.

In Fig. 15, the ratio $\bar{R}(\varphi_g)$,

$$\bar{R}(\varphi_g) = \frac{\Delta\nu^a(\varphi_g)}{\bar{\chi}_{C_3^m}^a} = \frac{\Delta\nu^e(\varphi_g)}{\bar{\chi}_{C_3^m}^e} \quad (25)$$

is plotted as a function of the crystal rotation angle φ_g . Clearly all six ratios $\bar{R}(\varphi_g)$ have the same dependence on φ_g , and the six curves in Fig. 15 may be superimposed by an appropriate shift along the φ_g axis. These identical dependences on φ_g confirm that only one dynamic species of cyclohexane is present in phase II, but that this species is present in six different orientations with respect to the crystal frame. The maxima of the curves shown in Fig. 15 correspond to the azimuthal orientation of the principal axis of the motionally averaged quadrupole coupling tensor.

We now consider the structural origin of the six different orientations of the motionally averaged quadrupole coupling tensors in phase II. First, the transition between the rhombohedral phase I and the monoclinic phase II is associated with crystal twinning to generate three orientation domains, which are related by a threefold axis collinear with the channel axis (see Fig. 16). Second, phase II is monoclinic with space group $P12_1/a1$ ($Z=4$). The four guest molecules in the unit cell are located at general positions and represent the same dynamic species. However, among the symmetry operations i , C_2 , and σ of the group, only pairs of molecules generated by applying the inversion (i) are indistinguishable by ^2H NMR, and the four molecules of the unit cell therefore give rise to two separate contributions to the spectrum. In total,

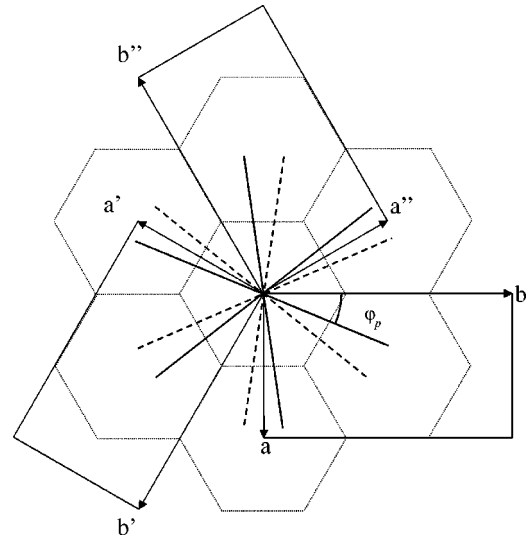


FIG. 16. View along the channel axis \vec{c}_m of the three equivalent ferroelastic domains. The dashed lines and solid lines represent the six directions of the principal axis of the motionally averaged quadrupole interaction tensor in phase II. φ_p is the angle between the \vec{b} axis and the projection of the principal axis of the motionally averaged quadrupole coupling tensor for one guest molecule.

we thus expect six separate contributions to the spectrum, arising from two orientations of the guest molecules in each of the three twin domains.

We now consider one guest molecule for which the projection of the principal axis of the motionally averaged quadrupole interaction tensor makes an angle φ_p with the reference axis \vec{b} (see Fig. 16). Because of the three monoclinic domains, the three orientations of this molecule (symbolized by solid lines in Fig. 16), give rise to the three contributions shown as solid lines in Fig. 15. The other three orientations of the guest molecule, obtained for example by applying C_2 rotation about the monoclinic axis \vec{b} in each domain, are represented by dashed lines in Fig. 16, and give rise to the three contributions shown as dashed lines in Fig. 15. The evolution of the possible solution φ_p as a function of temperature is reported in Table I, from which we note that φ_p evolves continuously in phase II on lowering the temperature.

By numerically calculating the theoretical values of \bar{R} and $\bar{\eta}$ defined by the eigenvalues of \bar{Q}_{II}^C , we have found that

TABLE I. Values of φ_p defining the azimuthal angle of the z axis of the motionally averaged quadrupole coupling tensor in phase II (145, 139, and 131 K) with respect to the reference axis \vec{b} . For the temperatures indicated with asterisks, the values of φ_p have been estimated by using the mean frequencies of the components constituting the split lines in phase III.

T (K)	φ_p (deg.)
145	15.9
139	20.8
131	24.7
123*	30
118*	30

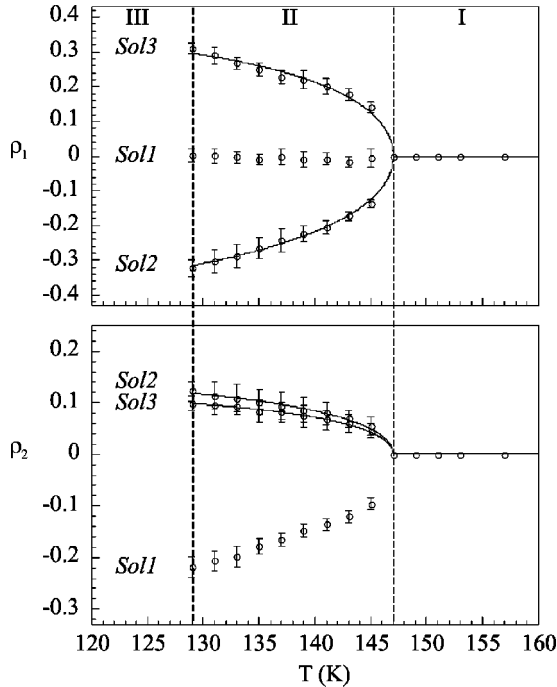


FIG. 17. Variation of the parameters ρ_1 (top) and ρ_2 (bottom) defined in the pseudospin model presented in the Appendix. The three possible solutions are denoted Sol1, Sol2, and Sol3 on each graph. These solutions couple (ρ_1, ρ_2) and provide values of \bar{R} and $\bar{\eta}$ within an error of 0.1% of the experimental values. Full lines represent the fits of $\rho_1(T)$ and $\rho_2(T)$ with relations (30) for Sol2 and Sol3.

several sets of solutions λ (solid lines in Fig. 13), ρ_1 and ρ_2 (Fig. 17) fit the experimental values of \bar{R} and $\bar{\eta}$ (Fig. 10) within an accuracy of 0.1%. As discussed above, the tilt angle is deduced to be around 60° in phase I, and we keep only those solutions that provide a continuous change of λ at the second order transition between phases I and II. As shown in Fig. 13, the tilt angle λ either remains approximately constant with a value close to 60° or decreases to reach a value of about 55° at the lowest temperatures in phase II. However, for each solution of the tilt angle, there are three solutions for the parameters ρ_1 and ρ_2 , denoted Sol1, Sol2, and Sol3 in Fig. 17. To analyze these three solutions, we have expressed the occupation probabilities defined in Eq. (A4) of the Appendix by using the parameters ρ_1 and ρ_2 [Eq. (23)]:

$$\begin{aligned} p_1 + p_5 &= \frac{1}{3} + (\rho_1 + \rho_2), \\ p_2 + p_6 &= \frac{1}{3} - 2\rho_2, \\ p_3 + p_4 &= \frac{1}{3} + (\rho_2 - \rho_1). \end{aligned} \quad (26)$$

Considering the solution Sol1 ($\rho_1 \approx 0$ and $\rho_2 < 0$), the varia-

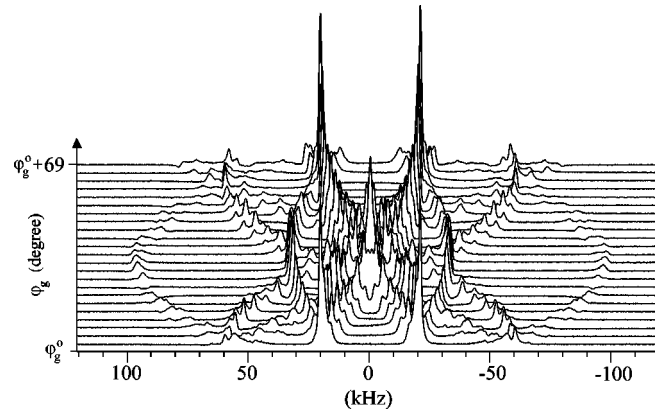


FIG. 18. Experimental single crystal ^2H NMR spectra recorded (with echo delay $30 \mu\text{s}$) for cyclohexane- d_{12} /thiourea in phase III at 118 K as a function of rotation (φ_g) of the crystal about the channel axis, with the channel axis perpendicular to the magnetic field \vec{B}_0 . The plot represents a total variation of 69° in the crystal orientation.

tions of ρ_1 and ρ_2 as a function of temperature are such that, on decreasing temperature, the probabilities of orientations 1, 3, 4, and 5 in Fig. 8 will decrease, whereas the probabilities of orientations 2 and/or 6 will increase [see Eq. (26)]. On the other hand, Fig. 17 shows that for solutions Sol2 and Sol3, the corresponding values of ρ_2 are identical within experimental accuracy whereas those of ρ_1 have opposite signs with the same absolute values. From Eq. (26), it clearly appears that solutions Sol2 and Sol3 are equivalent.

3. Phase III

The first order phase transition between phases II and III is clearly evident around 129 K (Figs. 9 and 10), and is associated with freezing out the reorientation of the C_3^m axis. Thus, the only motion effective on the ^2H NMR time scale in phase III is the reorientation of each guest molecule about its C_3^m axis and thus $\bar{R} = 1$ with $\bar{\eta} = 0$. At 129 K, the powder ^2H NMR spectrum in Fig. 9 clearly represents the superposition of two powder patterns, suggesting the coexistence of two dynamically different guest species. This observation may be explained by the coexistence of phases II and III across a temperature domain of about 4 K (the powder ^2H NMR spectrum recorded at 129 K resembles a superposition of those recorded at 131 and 127 K), associated with the first order character of the transition between phases II and III.

A stack plot of single crystal ^2H NMR spectra recorded as a function of crystal orientation in phase III (118 K) is shown in Fig. 18. In contrast to the spectra in phase II (Fig. 14), the lines observed in phase III are broad, with some structure, and may even be split into several components about a mean frequency. Several factors may contribute to these observations. First, we observed that on crossing the transition from phase II to phase III, the crystal develops some microcracks, which is not unexpected for a strongly first order phase transition. Thus, the crystal in phase III is actually a mosaic of very slightly misoriented crystallites. Second, it is plausible that freezing out the reorientation

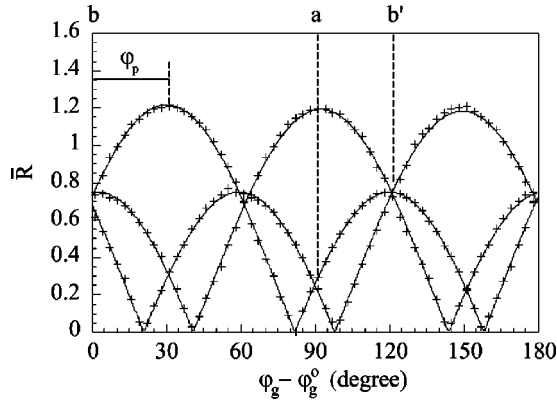


FIG. 19. Plot of $\bar{R}(\varphi_g)$ obtained from single crystal ^2H NMR data recorded (with echo delay $30\ \mu\text{s}$) at 118 K in phase III of cyclohexane- d_{12} /thiourea. On the top, the directions of the monoclinic axes are indicated for different twin domains, which differ in orientation by 120° in φ_g .

of the C_3^m axis of the guest molecules on crossing the phase transition may induce some static orientational disorder in phase III. Third, the single crystal ^2H NMR spectra recorded in phase III are often found to display phase distortions, probably caused by the virtual free induction decay or feedthrough signal that is not refocused by the second pulse in the quadrupole echo sequence.⁴⁰ Factors that may contribute to this effect include dipole-dipole interactions, which are expected to be stronger in phase III due to the lesser extent of dynamic averaging (a more detailed investigation into the fundamentals underlying the observed distortions will be the subject of a future study).

In a first level of approximation, we may consider the mean frequency of the components constituting the split lines in phase III. On this basis we have determined the ratio $\bar{R}(\varphi_g)$ defined in Eq. (23) and the results are shown in Fig. 19. The fact that $\bar{R}(\varphi_g)$ is invariant for the two temperatures studied in phase III supports our assertion that the C_3^m axes of the guest molecules do not undergo reorientational motion (on the ^2H NMR time scale) in phase III. The observation of three essentially identical curves separated by offsets of around 120° in φ_g arises due to the effects of crystal twinning, as discussed above for phase II. Since the space group of phase III is $P12_1/a1$ (as in phase II), we may expect to observe separate contributions to the spectrum from the two guest molecules in the unit cell related by the twofold symmetry axis. In this case, however, the contributions of these molecules to the spectrum are superimposed because of the particular value taken by φ_p (in Table I, $\varphi_p = 30^\circ$ in phase III), i.e., the contributions symbolized by dashed lines and solid lines in Fig. 16 for phase II are superimposed in phase III.

D. Discussion

In summary, our single crystal and powder ^2H NMR experiments have shown that in phase I, the motionally averaged quadrupole coupling tensor is axially symmetric, in agreement with previous studies.^{14,15} On crossing the transi-

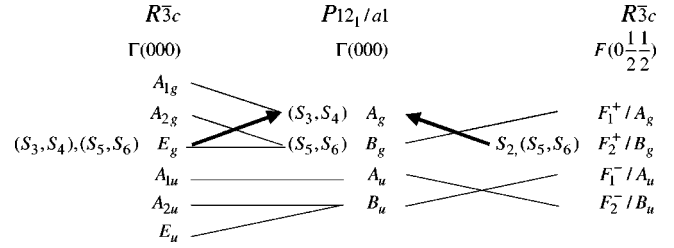


FIG. 20. Compatibility relations between the $R\bar{3}c$ space group representations at points $F(0\frac{1}{2}\frac{1}{2})$ and $\Gamma(000)$ of phase I with those of the $P12_1/a1$ space group at the zone center of phase II.

tion temperature from phase I to phase II, the C_3 symmetry axis of the $R\bar{3}c$ space group is lost, and the motionally averaged quadrupole coupling tensor is no longer axially symmetric. These single crystal ^2H NMR experiments demonstrate clearly that there is only one type of dynamic species of guest molecule in phase II, in contrast with interpretations proposed previously.¹⁵ Our single crystal ^2H NMR spectra probe very precisely the relative orientations of the guest molecules, which may be explained on the basis of the site symmetry properties of the structure and proposed modes of crystal twinning. In phase III, the orientation of the C_3^m axis of each guest molecule becomes fixed relative to the host structure. In all phases, there is rapid reorientation of each cyclohexane guest molecule about its C_3^m axis.

The multidimensional pseudospin approach presented above is not sufficient to draw a definitive conclusion concerning the mechanism of the transition between phases I and II. Indeed, instead of considering s_j in an isolated site, the pseudospin variables (hereafter denoted S_j) must be determined in the space group symmetry, as described in the Appendix. As the transition between phases I and II is essentially characterized by a doubling of the unit cell, we must consider cyclohexane sites in two primitive rhombohedral unit cells of phase I in order to describe the collective effect in terms of a multidimensional pseudospin model. The compatibility relations between specified zone points of phases I and II allow the determination of the collective pseudospin variables S_j behaving as order parameters (Fig. 20). Finally, we find that the four cyclohexane molecules of the monoclinic unit cell of phase II undergo jumps among six orientations (according to the orientation labels of Fig. 8) with the two probability distributions given in Eq. (A7) of the Appendix. There are two distributions of the p_i values related to each other by the 2_1 screw axis parallel to the monoclinic \vec{b}_m direction, on the one hand corresponding to cyclohexane molecules in positions $k=1, 2$ and on the other hand corresponding to cyclohexane molecules in positions $k=3, 4$. From these two probability distributions, we calculate the same motionally averaged quadrupole coupling constants $\bar{\chi}$ and motionally averaged asymmetry parameters $\bar{\eta}$, in agreement with the experimental results which show that only one dynamic species is observed in phase II. However, following the pseudospin model, the theoretical ratio $\bar{R}(\varphi_g)$ [see Eq. (25)] for single crystal ^2H NMR data is given by

TABLE II. Scale factors a_i and b_i obtained by fitting the experimental values of the parameters $\rho_1(T)$ and $\rho_2(T)$ presented as solutions Sol2 and Sol3. Res. is the standard definition of the residual sum of squares in the least-squares method.

	a_1	b_1	a_2	b_2	Res.
Sol2	-1.15 ± 0.05	0.72 ± 0.16	0.47 ± 0.03	-0.37 ± 0.06	0.997
Sol3	1.18 ± 0.07	-0.98 ± 0.23	0.41 ± 0.03	-0.36 ± 0.04	0.996

$$\bar{R}(\varphi_g) = \frac{3}{2} \left| P_2(\cos \lambda) - \frac{9}{4} \sin^2 \lambda \left[\rho_2 \cos 2\varphi_c - \frac{1}{\sqrt{3}} \rho_1 \sin 2\varphi_c \right] \right|, \quad (27)$$

where $\varphi_c = \varphi_g - \varphi_g^\circ + i_d 2\pi/3$, and $i_d = 0, 1$ or 2 refers to the twin domain considered. The sign of ρ_1 depends on the position of the cyclohexane molecule in the unit cell (as in the Appendix, ρ_1 has a positive value for positions $k=1, 2$ and a negative value for positions $k=3, 4$). Considering Eq. (27), the z axis of the motionally averaged quadrupole coupling tensor has an azimuthal angle φ_p with respect to the monoclinic axis \vec{b}_m given by

$$\varphi_p = \left| \frac{1}{2} \arctan \left(\frac{1}{\sqrt{3}} \frac{\rho_1}{\rho_2} \right) \right|. \quad (28)$$

It clearly appears that if ρ_1 or ρ_2 is equal to zero in Eq. (28), φ_p remains constant as a function of temperature, in contradiction with the experimental values in Table I. Thus, solution Sol1 ($\rho_1 \approx 0$ and $\rho_2 < 0$) must be ruled out. This is not surprising as the value $\rho_1 \approx 0$ imposes a constraint on the relative amplitudes of s_4 and s_5 [see Eq. (23)] which is not determined by the symmetry properties of phase II (see the Appendix). In contrast, positive values of ρ_1 in Eq. (28) (i.e., solution Sol3) will fit the experimental $\bar{R}(\varphi_g)$ results shown in Fig. 15 as full lines, and negative values of ρ_1 (i.e., solution Sol2) will fit the experimental $\bar{R}(\varphi_g)$ results shown in Fig. 15 as dashed lines. Thus, solutions Sol2 and Sol3 represent the two probability distributions implied by the cyclohexane positions $k=1, 2$ and $k=3, 4$ in the monoclinic unit cell.

The assumption concerning the equivalence of solutions Sol2 and Sol3 is confirmed by the analysis of the temperature dependence of the parameters ρ_1 and ρ_2 . Indeed, the primary order parameter ζ which drives the second-order transition from phase I to phase II is a linear combination of S_2 , S_5 , and S_6 coordinates, whereas S_3 and S_4 behave as secondary order parameters (see the Appendix) i.e., they are proportional to ζ^2 . In Sec. III we have shown that the spontaneous strain components ($e_1 - e_2$) and e_5 , which characterize the distortion of the unit cell in phase II, are secondary order parameters and display a linear temperature dependence in phase II, as expected from classical Landau theory.²⁵ From Eq. (23), it appears that parameters ρ_1 and ρ_2 both contain primary (S_5 and S_6) and secondary (S_3 and S_4)

order parameter components. It follows that the expected temperature dependence of ρ_1 and ρ_2 according to Landau theory is

$$\rho_i = a_i \zeta + b_i \zeta^2 \quad (i=1,2) \quad (29)$$

where the order parameter ζ driving the transition from phase II to phase I is proportional to $[(T_{c1} - T)/T_{c1}]^{1/2}$, and a_i and b_i are amplitude factors. The experimental values of $\rho_1(T)$ and $\rho_2(T)$ have been fitted by means of Eq. (29) with $T_{c1} = 147$ K. The resulting values of the amplitudes a_i and b_i are presented in Table II and the comparison between the theoretical (full lines) and experimental (symbols) values of $\rho_1(T)$ and $\rho_2(T)$ is shown in Fig. 19. We note in Table II that for solutions Sol2 and Sol3, the amplitudes a_1 and b_1 describing the parameter ρ_1 have the same absolute values but opposite signs whereas the amplitudes a_2 and b_2 describing the parameter ρ_2 are equivalent, as expected from the pseudospin model. Thus, the temperature dependence of the parameters ρ_1 and ρ_2 fits well with classical Landau theory and so is fully consistent with independent measurements of the spontaneous strain components in phase II by means of x-ray diffraction.

The powder ^2H NMR data in phase III indicate that each cyclohexane guest molecule reorients about its C_3^m axis, and may be fitted by an N -site $2\pi/N$ jump model with $N=3$. Using this model, the ratio $\bar{R}(\varphi_g)$ becomes

$$\bar{R}(\varphi_g) = \frac{3}{2} |P_2(\sin \lambda \cos \varphi_c)|, \quad (30)$$

where $\varphi_c = \varphi_g - \varphi_g^\circ + \varphi_p + i_d 2\pi/3$. The experimental data (Fig. 19) have been fitted by means of the parameters λ and φ_p , from which we found $\lambda = 70^\circ$. For the value of φ_p , it was not possible to distinguish between $\varphi_p = 30^\circ$ and $\varphi_p = 90^\circ$ because of the crystal twinning and the properties of the quadrupole coupling tensor. Thus, the transition from phase II to phase III is characterized by a strong lattice distortion associated with an abrupt change in the tilt angle together with an abrupt orientational ordering of the C_3^m axis. In these respects, the transition from phase II to phase III exhibits some reconstructive character, and is thus clearly disconnected from the second-order transition from phase I to phase II.

V. CONCLUSIONS

The high-temperature phase I of the cyclohexane/thiourea inclusion compound is rhombohedral with space group

$R\bar{3}c$, as determined previously by Lenné¹⁰ from single crystal x-ray diffraction data. Probably because of crystal twinning and the use of single-crystal x-ray diffraction, Clément *et al.*⁹ did not report the space groups of the two low-temperature phases (phases II and III) of the inclusion compound. By using the high resolution provided by synchrotron x-ray powder diffraction data, we have been able to assign the space groups of both phases II and III as $P12_1/a1$. Moreover by analyzing the experimental data, we determine that the phase transition occurring at T_{c1} has all the continuous characteristics of a second-order phase transition, whereas the transition occurring at T_{c2} has the characteristics of a first order phase transition. We have shown that the second-order transition at T_{c1} is well described by means of a simple Landau potential developed up to the fourth order. The transition at T_{c2} is disconnected from the transition at T_{c1} .

The work reported in this paper illustrates the fact that single crystal ²H NMR spectroscopy is a powerful probe for understanding the relationship between the dynamic behavior of the guest molecules and the host crystal structure in the cyclohexane/thiourea inclusion compound. In particular, we have shown that simple jump models (i.e., multidimensional pseudospin models) elaborated by a detailed consideration of the symmetry properties of the composite crystal are sufficient to interpret the ²H NMR data in all three phases of the inclusion compound.

In phase I, the disorder of the guest molecules can be described in terms of a model of jumps of the molecular C_3^m axis between six equiprobable orientations according to the D_3 point group symmetry of the site, together with rapid reorientation of each molecule about its C_3^m axis. In phase II, however, dynamic disorder of the cyclohexane guest molecules must be interpreted in terms of reorientation among six inequivalent orientations, although with specific relationships between these orientations. Order parameters driving the transition from phase I to phase II have been identified and the orientational ordering process in phase II has been discussed. In particular, we have shown that the temperature dependence of both primary and secondary order parameters in phase II fits well with classical Landau theory. The main reason for the ability of such a simple development of the free energy to account for the complex ordering processes occurring in phase II lies in the fact that long-range interactions strongly dominate over short-range forces (which could induce local fluctuations of the order parameters). Indeed, these long-range elastic interactions, which are probably related to the hydrogen bonding network of the thiourea host substructure and which are responsible for the macroscopic spontaneous strains (improper ferroelastic transition), may be expected to control the ordering processes governed essentially by short-range van der Waals forces in the guest substructure.

The transition from phase II to phase III is strongly of first order and exhibits some reconstructive character. An abrupt ordering in the orientation of the C_3^m axis of the cyclohexane molecules takes place in phase III, due to freezing the motions of this axis relative to the host structure. However,

rapid reorientation of each cyclohexane molecule about its C_3^m axis still persists in phase III.

These results provide important information required to elaborate a microscopic model for the phase transition sequence in the cyclohexane/thiourea inclusion compound. However, it is important to emphasize that these ²H NMR experiments have not provided any information on the time scales for the reorientational processes, except that the motions discussed are effective on a time scale shorter than approximately 10^{-7} s. More detailed information on the time scales of the dynamic processes on these shorter time scales can be obtained by combining molecular dynamics simulations and incoherent quasielastic neutron scattering experiments,^{35,36,41} as well as by measurement and analysis of ²H NMR spin-lattice relaxation times.

ACKNOWLEDGMENTS

We are grateful to Daresbury Laboratory for the provision of beam time for powder x-ray diffraction, and to Dr. B.M. Kariuki and Dr. E.J. MacLean for experimental assistance. The British Council, NATO, the “Ministère des affaires étrangères” (collaborative research grants to F.G. and K.D.M.H.) and the regions of Aquitaine and Euskadi (collaborative research grant to F.G. and E.H.B.), are thanked for financial support. We thank Dr. Marta Bach for her considerable help during the recording of powder ²H NMR spectra, and Professor P. Graveriau and M. Lebraud for assistance in the single crystal x-ray diffraction experiment.

APPENDIX: DESCRIPTION OF ORDER PARAMETERS WITH A MULTIDIMENSIONAL PSEUDO-SPIN MODEL

1. Individual reorientations

The Frenkel model, used to describe order-disorder processes and phase transitions in terms of guest molecule dynamics, is based on probability variations δp_i of each guest molecule orientation i . Thus, the probability p_i for the orientation i is given by

$$p_i = \frac{1}{6} + \delta p_i \quad (i=1, \dots, 6). \quad (\text{A1})$$

The site symmetry group D_3 of the guest molecules in the disordered phase I allows the six pseudospin coordinates s_j to be determined with the projection operators method

$$s_j = \sum_i M_{ij} \delta p_i \quad (i=1, \dots, 6), \quad (\text{A2})$$

where M_{ij} are the elements of the unitary transformation matrix \mathbf{M} , generated by the three irreducible representations A_1 , A_2 , and E of the D_3 group. The matrix \mathbf{M} is given by

$$\mathbf{M} = \begin{pmatrix} \frac{1}{\sqrt{6}} & \frac{1}{\sqrt{6}} & \frac{1}{\sqrt{6}} & \frac{1}{\sqrt{6}} & \frac{1}{\sqrt{6}} & \frac{1}{\sqrt{6}} \\ \frac{1}{\sqrt{6}} & \frac{1}{\sqrt{6}} & \frac{1}{\sqrt{6}} & -\frac{1}{\sqrt{6}} & -\frac{1}{\sqrt{6}} & -\frac{1}{\sqrt{6}} \\ \frac{2}{\sqrt{12}} & -\frac{1}{\sqrt{12}} & -\frac{1}{\sqrt{12}} & \frac{2}{\sqrt{12}} & -\frac{1}{\sqrt{12}} & -\frac{1}{\sqrt{12}} \\ 0 & -\frac{1}{2} & \frac{1}{2} & 0 & -\frac{1}{2} & \frac{1}{2} \\ \frac{2}{\sqrt{12}} & -\frac{1}{\sqrt{12}} & -\frac{1}{\sqrt{12}} & -\frac{2}{\sqrt{12}} & \frac{1}{\sqrt{12}} & \frac{1}{\sqrt{12}} \\ 0 & \frac{1}{2} & -\frac{1}{2} & 0 & -\frac{1}{2} & \frac{1}{2} \end{pmatrix}. \quad (\text{A3})$$

Thus, the occupation probabilities p_i obtained under the action of the pseudospin coordinates s_j are given by

$$p_1 = \frac{1}{6} + \frac{1}{\sqrt{6}}s_1 + \frac{1}{\sqrt{6}}s_2 + \frac{2}{\sqrt{12}}s_3 + \frac{2}{\sqrt{12}}s_5,$$

$$p_2 = \frac{1}{6} + \frac{1}{\sqrt{6}}s_1 + \frac{1}{\sqrt{6}}s_2 - \frac{1}{\sqrt{12}}s_3 - \frac{1}{2}s_4 - \frac{1}{\sqrt{12}}s_5 + \frac{1}{2}s_6,$$

$$p_3 = \frac{1}{6} + \frac{1}{\sqrt{6}}s_1 + \frac{1}{\sqrt{6}}s_2 - \frac{1}{\sqrt{12}}s_3 + \frac{1}{2}s_4 - \frac{1}{\sqrt{12}}s_5 - \frac{1}{2}s_6,$$

$$p_4 = \frac{1}{6} + \frac{1}{\sqrt{6}}s_1 - \frac{1}{\sqrt{6}}s_2 + \frac{2}{\sqrt{12}}s_3 - \frac{2}{\sqrt{12}}s_5,$$

$$p_5 = \frac{1}{6} + \frac{1}{\sqrt{6}}s_1 - \frac{1}{\sqrt{6}}s_2 - \frac{1}{\sqrt{12}}s_3 - \frac{1}{2}s_4 + \frac{1}{\sqrt{12}}s_5 - \frac{1}{2}s_6,$$

$$p_6 = \frac{1}{6} + \frac{1}{\sqrt{6}}s_1 - \frac{1}{\sqrt{6}}s_2 - \frac{1}{\sqrt{12}}s_3 + \frac{1}{2}s_4 + \frac{1}{\sqrt{12}}s_5 + \frac{1}{2}s_6. \quad (\text{A4})$$

From the condition $\sum_{i=1}^6 p_i = 1$, it follows that $s_1 = 0$ (identity). In contrast, all other s_j ($j \neq 1$) are symmetry breaking coordinates, so that order parameters expressed in terms of the occupation probabilities are

$$s_2 = \frac{1}{\sqrt{6}}(p_1 + p_2 + p_3 - p_4 - p_5 - p_6),$$

$$s_3 = \frac{1}{\sqrt{12}}(2p_1 - p_2 - p_3 + 2p_4 - p_5 - p_6),$$

$$s_4 = \frac{1}{2}(-p_2 + p_3 - p_5 + p_6),$$

$$s_5 = \frac{1}{\sqrt{12}}(2p_1 - p_2 - p_3 - 2p_4 + p_5 + p_6),$$

$$s_6 = \frac{1}{2}(p_2 - p_3 - p_5 + p_6). \quad (\text{A5})$$

In the case of the transformation from phase I to phase II, in which the site symmetry of the guest molecule is lowered from D_3 to C_1 (general position), all coordinates s_j ($j \neq 1$) are involved as order parameters, since they all induce the identity representation of C_1 point group. An orientationally ordered state can be achieved only when particular values are imposed on the relative amplitudes of the different order parameters. For example, the ordered state $p_1 = 1$ with $p_i = 0$ ($i \neq 1$) corresponds to $s_2 = 1/\sqrt{6}$, $s_3 = s_5 = 1/\sqrt{3}$, and $s_4 = s_6 = 0$. In fact, such constraints are not imposed by the symmetry properties of phase II, so that at a given temperature, all occupation probabilities $p_i \neq \frac{1}{6}$ are expected to be different from each other.

2. Collective effect: Description of pseudospin coordinates in the space group

In order to account for the doubling of the unit cell at the phase transition from $R\bar{3}c$ ($Z=2$) to $P12_1/a1$ ($Z=4$), we

must consider the four cyclohexane guest molecules in the monoclinic unit cell. The positions of these guest molecules referred to the space group $R\bar{3}c$ (primitive rhombohedral setting) are

-
- site 1: position $(\frac{1}{4}, \frac{1}{4}, \frac{1}{4})$,
- site 2: position $(\frac{3}{4}, \frac{3}{4}, \frac{3}{4})$ deduced from site 1 by the inversion $\{i|000\}$,
- site 3: deduced from site 1 by the translation $\{E|010\}$,
- site 4: deduced from site 2 by the translation $\{E|010\}$.
-

As established in this paper, point $F(0 \frac{1}{2} \frac{1}{2})$ located at the surface of the rhombohedral Brillouin zone becomes a zone-center point in the monoclinic reciprocal space. The compatibility relations between the $R\bar{3}c$ space group representations at points $F(0 \frac{1}{2} \frac{1}{2})$ and $\Gamma(000)$ with those of the $P12_1/a1$ space group at the zone center are shown in Fig. 20. It turns out that the primary order parameter belongs to the F_2^+/B_g space group representation whereas the representation E_g at the zone center is associated with a secondary order parameter. Hence, the relevant pseudospin coordinates S_j ($j \neq 1$) developed according to the space group representations F_2^+ and E_g on the basis of the site coordinates s_j^k are of the form

$$\begin{aligned} S_2(F_2^+) &= s_2^1 + s_2^2 - s_2^3 - s_2^4, \\ S_3(E_g) &= s_3^1 + s_3^2 + s_3^3 + s_3^4, \\ S_4(E_g) &= s_4^1 + s_4^2 + s_4^3 + s_4^4, \\ S_5(F_2^+) &= s_5^1 + s_5^2 - s_5^3 - s_5^4, \\ S_6(F_2^+) &= -s_6^1 - s_6^2 + s_6^3 + s_6^4, \end{aligned} \quad (\text{A6})$$

where the superscript $k=1, \dots, 4$ refers to the site label specified above.

Thus, we establish that all coordinates S_j ($j=2, \dots, 6$) and consequently all of the corresponding s_j^k are order parameters for the transition between phases I and II (see Appendix A. Furthermore, we learn that S_2 , S_5 , and S_6 (and so s_2^k , s_5^k , and s_6^k) with F_2^+ symmetry behave as primary order parameters, and that S_3 and S_4 (and so s_3^k and s_4^k) are secondary order parameters. Then, the occupation probabilities of the cyclohexane molecules p_i^k in the different sites are such that

$$\begin{aligned} p_1^1 &= p_1^2 = p_4^3 = p_4^4, \\ p_2^1 &= p_2^2 = p_6^3 = p_6^4, \\ p_3^1 &= p_3^2 = p_5^3 = p_5^4, \\ p_4^1 &= p_4^2 = p_1^3 = p_1^4, \\ p_5^1 &= p_5^2 = p_3^3 = p_3^4, \\ p_6^1 &= p_6^2 = p_2^3 = p_2^4. \end{aligned} \quad (\text{A7})$$

This means that there are two distributions of p_i values, corresponding to sites 1 and 2 on the one hand and sites 3 and 4 on the other hand, and related to each other by the 2_1 screw axis parallel to the monoclinic \vec{b}_m direction.

¹M. D. Hollingsworth and K. D. M. Harris, in *Comprehensive Supramolecular Chemistry*, edited by J. L. Atwood, J. E. D. Davies, D. D. MacNicol, and F. Vögtle (Pergamon Press, Oxford, 1996), Vol. 6, p. 177.

²K. D. M. Harris, *Chem. Soc. Rev.* **26**, 279 (1997).

³K. D. M. Harris, *J. Chin. Chem. Soc. (Taipei)* **46**, 5 (1999).

⁴F. Guillaume, *J. Chim. Phys.* **96**, 1295 (1999).

⁵R. Lefort, J. Etrillard, B. Toudic, F. Guillaume, T. Breczewski, and P. Bourges, *Phys. Rev. Lett.* **77**, 4027 (1996).

⁶H. Le Lann, C. Odin, J. C. Ameline, B. Toudic, J. Gallier, F.

Guillaume, and T. Breczewski, *Phys. Rev. B* **62**, 5442 (2000).

⁷J. Ollivier, C. Ecolivet, S. Beaufils, F. Guillaume, and T. Breczewski, *Europhys. Lett.* **43**, 546 (1998).

⁸J. Etrillard, J.C. Lasjaunias, B. Toudic, F. Guillaume, and T. Breczewski, *Europhys. Lett.* **49**, 610 (2000).

⁹R. Clément, C. Mazières, M. Gourdj, and L. Guibé, *J. Chem. Phys.* **67**, 5381 (1977).

¹⁰H.-U. Lenné, *Acta Crystallogr.* **7**, 1 (1954).

¹¹E. K. H. Salje, in *Phase Transitions in Ferroelastic and Coelastic Crystals* (Cambridge University Press, Cambridge,

- 1990).
- ¹²M. J. Jones, I. J. Shannon, and K. D. M. Harris, *J. Chem. Soc., Faraday Trans.* **92**, 273 (1996).
- ¹³R. Clément, M. Gourdjji, and L. Guibé, *Mol. Phys.* **21**, 247 (1971).
- ¹⁴E. Meirovitch, T. Krant, and S. Vega, *J. Phys. Chem.* **87**, 1390 (1983).
- ¹⁵R. Poupko, E. Fourman, K. Müller, and Z. Luz, *J. Phys. Chem.* **95**, 407 (1991).
- ¹⁶J. H. Davis, K. R. Jeffery, M. Bloom, M. I. Valic, and T. P. Higgs, *Chem. Phys. Lett.* **42**, 390 (1976).
- ¹⁷A. J. Vega and Z. Luz, *J. Chem. Phys.* **86**, 1803 (1987).
- ¹⁸R. Clément, J. Jegoudez, and C. Mazières, *J. Solid State Chem.* **10**, 46 (1974).
- ¹⁹K. D. M. Harris, *J. Solid State Chem.* **84**, 280 (1990).
- ²⁰N. R. Kunchur and M. R. Truter, *J. Chem. Soc.* **517**, 2551 (1958).
- ²¹M. R. Truter, *Acta Crystallogr.* **22**, 556 (1967).
- ²²R. Kahn, R. Fourme, D. André, and M. Renaud, *Acta Crystallogr., Sect. B: Struct. Crystallogr. Cryst. Chem.* **29**, 131 (1973).
- ²³H. T. Stokes and D. M. Hatch, in *Isotropy Subgroups of the 230 Crystallographic Space Groups* (World Scientific, Singapore, 1988).
- ²⁴C. J. Bradley and A. P. Cracknell, in *The Mathematical Theory of Symmetry in Solids* (Clarendon Press, Oxford, 1972).
- ²⁵J. C. Toledano and P. Toledano, in *The Landau Theory of Phase Transitions* (World Scientific, Singapore, 1987).
- ²⁶J. F. Nye, in *Physical Properties of Crystals* (Oxford University Press, Oxford, England, 1957).
- ²⁷Yu. M. Gufan, in *Structural Phase Transitions* (Nauka, Moscow, 1982).
- ²⁸Y. A. Izyumov and V. N. Syromyatnikov, in *Phase Transitions and Crystal Symmetry* (Kluwer, Dordrecht, 1990).
- ²⁹Y. Ishibashi and Y. Hidaka, *J. Phys. Soc. Jpn.* **60**, 1634 (1991).
- ³⁰R. J. Wittebort, E. T. Olejniczak, and R. G. Griffin, *J. Chem. Phys.* **86**, 5411 (1987).
- ³¹M. Mehring, in *Principles of High Resolution NMR in Solids* (Springer-Verlag, Berlin, 1983).
- ³²R. Blinc, B. Zeks, and R. Kind, *Phys. Rev. B* **17**, 3409 (1978).
- ³³R. Kind, R. Blinc, and B. Zeks, *Phys. Rev. B* **19**, 3743 (1979).
- ³⁴M. Couzi, P. Negrier, H. Poulet, and R. Pick, *Croat. Chem. Acta* **61**, 649 (1988).
- ³⁵A. Desmedt, Ph.D. thesis, University of Bordeaux I, France, 2001.
- ³⁶J. C. Soetens, A. Desmedt, F. Guillaume, and K. D. M. Harris, *Chem. Phys.* **261**, 125 (2000).
- ³⁷M. J. Jones, F. Guillaume, K. D. M. Harris, A. E. Aliev, P. Girard, and A. J. Dianoux, *Mol. Phys.* **93**, 545 (1998).
- ³⁸D. A. Dixon and A. Komornicki, *J. Phys. Chem.* **94**, 5630 (1990).
- ³⁹E. Bialkowska-Jaworska, M. Jaworski, and Z. Kisiel, *J. Mol. Struct.* **350**, 247 (1995).
- ⁴⁰U. Haerberlen (private communication).
- ⁴¹A. Desmedt, F. Guillaume, J. Combet, and A. J. Dianoux, *Physica B* (to be published).